ASTROBIOLOGY
Volume 00, Number 00, 2025

DOI: 10.1089/ast.2024.0034

Open camera or QR reader and scan code to access this article and other resources online.

# Photochemical Evolution of Alanine in Association with the Martian Soil Analog Montmorillonite: Insights Derived from Experiments Conducted on the International Space Station

Severin Wipf,[1] Paul Mabey,[1] Riccardo G. Urso,[2] Sebastian Wolf,[1] Arthur Stok,[3] Antonio J. Ricco,[4] Richard C. Quinn,[4] Andrew L. Mattioda,[4] Nykola C. Jones,[5] Søren V. Hoffmann,[5] Hervé Cottin,[6] Didier Chaput,[7] Pascale Ehrenfreund,[8,9] and Andreas Elsaesser[1]



**Abstract**

The *Photochemistry on the Space Station* (PSS) experiment was part of the European Space Agency's *EXPOSE-R2* mission and was conducted on the International Space Station from 2014 to 2016. The PSS experiment investigated the properties of montmorillonite clay as a protective shield against degradation of organic compounds that were exposed to elevated levels of ultraviolet (UV) radiation in space. Additionally, we examined the potential for montmorillonite to catalyze UV-induced breakdown of the amino acid alanine and its potential to trap the resulting photochemical byproducts within its interlayers. We tested pure alanine thin films, alanine thin films protected from direct UV exposure by a thin cover layer of montmorillonite, and an intimate combination of the two substances forming an organoclay. The samples were exposed to space conditions for 15.5 months and then returned to Earth for detailed analysis. Concurrent ground-control experiments subjected identical samples to simulated solar light irradiation. Fourier-transform infrared (FTIR) spectroscopy quantified molecular changes by comparing spectra obtained before and after exposure for both the space and ground-control samples. To more deeply understand the photochemical processes influencing the stability of irradiated alanine molecules, we performed an additional experiment using time-resolved FTIR spectroscopy for a second set of ground samples exposed to simulated solar light. Our collective experiments reveal that montmorillonite clay exhibits a dual, configuration-dependent effect on the stability of alanine: while a thin cover layer of the clay provides UV shielding that slows degradation, an intimate mixture of clay and amino acid hastens the photochemical decomposition of alanine by promoting certain chemical reactions. This observation is important to understand the preservation of amino acids in specific extraterrestrial environments, such as Mars: cover mineral layer depths of several millimeters are required to effectively shield organics from the harmful effects of UV radiation. We also explored the role of carbon dioxide ($CO_2$), a byproduct of alanine photolysis, as a tracer of the amino acid. $CO_2$ can be trapped within clay interlayers, particularly in clays with small interlayer ions such as sodium. Our studies emphasize the multifaceted interactions between montmorillonite clay and alanine under nonterrestrial conditions; thus, they contribute valuable

[1]Experimental Biophysics and Space Sciences, Department of Physics, Freie Universitaet Berlin, Berlin, Germany.
[2]INAF-Osservatorio Astrofisico di Catania, Catania, Italy.
[3]Faculty of Earth and Life Sciences, Vrije Universiteit Amsterdam, Amsterdam, The Netherlands.
[4]NASA Ames Research Center, Moffett Field, California, USA.
[5]Department of Physics and Astronomy, ISA, Aarhus University, Aarhus, Denmark.
[6]Univ Paris Est Creteil and Université Paris Cité, France.
[7]Centre Spatial de Toulouse, Centre National d'Etudes Spatiales (CNES), Toulouse cedex 9, France.
[8]Space Policy Institute, George Washington University, Washington, District of Columbia, USA.
[9]Laboratory for Astrophysics, Leiden Observatory, Leiden University, Leiden, The Netherlands.

insights to broader astrobiological research questions. Key Words: Alanine—Montmorillonite clay—UV radiation—Spectroscopy—Mars—Carbon dioxide. Astrobiology 00, 000–000.

## 1. Introduction

The search for traces of extant or extinct life within the solar system encompasses a variety of distinct environments (Barnes et al., 2021; Glaze et al, 2018; Grasset et al, 2013; Howell and Pappalardo, 2020; MacKenzie et al., 2021), with Mars of particular interest (Enya et al., 2022; Sephton and Carter, 2015). Our scientific understanding of its geological and environmental conditions is expanding, driven by the potential of direct biosignature identification by past, present, and future Mars missions (Bhartia et al., 2021; Bish et al., 2013; Morris et al., 2004; Rossi and van Gasselt, 2010). Nonetheless, the combination of atmospheric and geological composition, extreme temperatures, pressure, and radiation renders Mars and other planetary surfaces disadvantageous for the preservation of traces of life. This creates the risk that, even when organic compounds are found in such environments, they may bear little resemblance to the original molecular biosignatures as, for example, ultraviolet (UV) radiation can alter molecular identities by breaking and/or rearranging chemical bonds, and it can even induce ionization. Such processes can break down organic compounds within a matter of hours to days (Dartnell, 2011; Poch et al., 2014; Rak et al., 2015). Furthermore, solar charged particles and cosmic rays detrimentally impact organic compounds; this underscores the importance of radiation attenuation mechanisms in long-duration organic compound stability. Given that numerous extraterrestrial inorganic materials can serve as radiation shields, the geological environment is widely recognized as a critical factor that influences the stability of organic molecules (Hassler et al., 2014; Kopacz et al., 2023).

Laboratory experiments can elucidate the mechanisms of radiation interactions of organic compounds with inorganic materials. Purpose-built experimental setups can replicate certain physical and chemical parameters of extraterrestrial environments and facilitate systematic and time-effective characterization of multiple processes and sample types. However, the simulation of UVC radiation, especially at wavelengths shorter than 200 nm, proves challenging, and the effects of microgravity and the full range of energetic, charged particles remain elusive to laboratory replication (Cottin et al., 2017). Consequently, the combination of laboratory simulations and space experiments is a valuable tool that contributes key findings to our understanding of nonterrestrial environmental effects and to ongoing and future space missions. This synergy offers important insights for the selection of astrobiologically relevant molecular target signatures, as well as the interpretation of scientific findings. Previous space experiments, conducted aboard the International Space Station (ISS) and other space-based facilities, have provided important insights into the radiation-related chemical processes involving potential prebiotic molecules. These studies have also furnished knowledge essential for present and future space experiments (Bertrand et al., 2012; Bertrand et al., 2015; Ehrenfreund et al., 2014; Mattioda et al., 2012; Rabbow et al., 2015; Rabbow et al., 2012). The European Space Agency's *EXPOSE-R2* experiment was attached to the outside of the ISS from 2014 to 2016, where it exposed over 750 biological and chemical samples to space conditions for 15.5 months in low Earth orbit (LEO) (Rabbow et al., 2017). Within this framework, the *Photochemistry on the Space Station* experiment investigated the photochemical stability of several potential biosignatures when they were subjected to space conditions (Baratta et al., 2019; Cottin and Rettberg, 2019; Stalport et al., 2019). Concurrently, a laboratory control experiment, which employed an identical set of samples and utilized simulated solar irradiation, was conducted at the Microgravity User Support Center (MUSC) of the German Aerospace Center (DLR) in Cologne, Germany (Rabbow et al., 2017). After their exposure on the ISS and in the ground-based experiment, the samples underwent an in-depth laboratory analysis. In addition, we replicated the ground-control experiment, integrating time-resolved spectroscopy at 10-h intervals. The dataset derived from these *in situ* measurements provides an enhanced understanding of the photochemical stability of the proteinogenic amino acid alanine when it is combined with the inorganic phyllosilicate montmorillonite clay. Alanine is one of the simplest amino acids and supports essential functions in all living organisms (Higgs and Pudritz, 2009). Clay minerals, with their proclivity to adsorb organic compounds onto their surface or, in some cases, intercalate molecules between their layers, can catalyze polymerization of adsorbed organics (Brack, 2013); such processes are believed to have played a crucial role in the early formation of proteins from amino acids. Moreover, it has been suggested that structural anomalies within the bulk of clays might prompt the replication of specific polymer sequences and that organoclays might even exert stereoselective influences on amino acid stability (Brack, 2013; Valaskova and Martynkova, 2012). In the realm of endogenous synthesis theories, it is hypothesized that the clay minerals played a major role when assemblies of biomolecules formed primitive cells (Ferris, 2006; Kloprogge and Hartman, 2022). Clay's pertinence extends to Mars due to its abundance on the martian surface (Chyba and Sagan, 1992; Murchie et al., 2009); indeed, montmorillonite is frequently employed as a mineral clay surrogate for Mars in simulation experiments (Böttger et al., 2012; Primm et al., 2018). Paradoxically, alongside their potential to shield amino acids such as alanine from UV radiation, clays might hasten or amplify photodegradative effects due to their ability to catalyze polymerization via their large inner surfaces and charge-carrier transport capabilities (dos Santos et al., 2016). Our array of sample specimens helped us scrutinize how montmorillonite layers might protect alanine molecules from solar UV radiation. We also probed whether intercalation between the mineral layers augments alanine stability, and we explored the possible formation of stable byproducts. The results reported here contribute to the understanding of alanine's potential stability in the particular context of its interaction with montmorillonite.

## 2. Materials and Methods

The analyzed samples were prepared to replicate scenarios on extraterrestrial surfaces or in subsurface regions such as those found on Mars. To investigate the UV-shielding impact of clays, an alanine thin film was applied atop a layer of clay, and the sample was subsequently oriented such that the clay faced the UV illumination directly, thus shielding the amino acid. To understand the intrinsic photochemical stability of alanine when it is in more intimate contact with clay (and without an uninterrupted shielding layer between UV and alanine), an alanine-montmorillonite organoclay was prepared. In addition to the *EXPOSE-R2* experiment and its ground controls, a supplementary laboratory experiment was conducted that involved the irradiation of analogous samples with simulated solar UV illumination, accompanied by the acquisition of time-resolved spectra. In both experiments, the samples were analyzed via Fourier-transform infrared (FTIR) absorption spectroscopy to evaluate the degradation of specific chemical bonds and functional groups within alanine.

### 2.1. Hardware and timeline

All samples within the *EXPOSE-R2* facility were positioned in compartments measuring 77 mm × 83 mm × 33.5 mm. These compartments were then integrated into the *EXPOSE-R2* monoblock, which featured a UV and particle sensor. A schematic representation of the sample compartments is presented in the left column of Fig. 1. The compartment exposed to the Sun (*ISS exposed*, depicted in blue) was subjected to UV radiation, whereas an adjacent compartment (*ISS dark*, illustrated in purple) was situated beneath the exposed compartment and thus screened from electromagnetic radiation. These screened samples served as dark control counterparts that allowed assessment of the degradation effects resulting from temperature variation and particle radiation separately. On July 23, 2014, the space hardware was launched from Baikonur, Kazakhstan, and subsequently affixed to the ISS Zvezda Module's exterior on August 18, 2014. This marked the start of exposure to the space environment. The corresponding ground-control experiment, conducted at MUSC, replicated temperature fluctuations and irradiation with wavelengths longer than approximately 200 nm, based on telemetry data obtained from the space experiment. The ground-control experiment employed identical compartments: one was exposed to simulated solar light in the UV-Vis region (referred to as *ground exposed*), whereas another was positioned beneath (termed *ground dark*) and served as dark control samples. An additional compartment (not depicted) remained at a constant temperature of 5°C within a dark environment throughout the duration of the experiment and functioned as a reference set. Comprehensive details concerning hardware, the timeline, environmental parameters, and sample species for the other *EXPOSE-R2* experiments

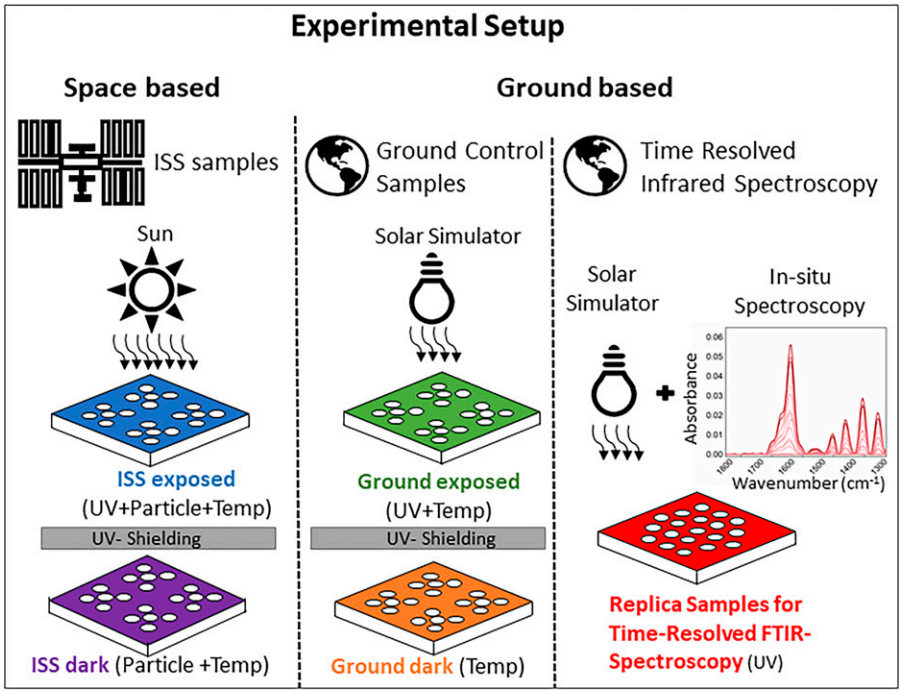


**FIG. 1.** Schematic illustrations depicting the sample compartments of the ISS experiment, the ground-control experiment, and the time-resolved spectroscopy experiment. In the left column: The ISS experiment includes both the ISS-exposed samples (subjected to UV radiation, particle radiation, and temperature fluctuations) and the ISS dark samples (protected from light but exposed to particle radiation and temperature variations). In the center column: Within the ground experiment at MUSC, the ground-exposed samples underwent simulated solar light and temperature conditions, while the ground dark samples were subjected solely to the temperature profile. In the right column: For time-resolved spectroscopy, the sample species were subjected to solar-simulator irradiation and analyzed using FTIR spectroscopy at 10-h intervals. The color-coded system employed in the schematic illustration of the sample compartments within this figure corresponds to the respective sample sets in the presentation of the results. FTIR, Fourier-transform infrared; ISS, International Space Station; MUSC, Microgravity User Support Center; UV, ultraviolet.

can be found in Rabbow et al. (2017). The time measurement series experiment was executed within a 99.999% high-purity nitrogen atmosphere of a glovebox, which emulated the experimental conditions of the ground-exposed samples at MUSC.

### 2.2. Radiation and temperature

To estimate the electromagnetic radiation profile received by the ISS-exposed samples, simulation data were employed, assuming the AM0 solar spectrum in LEO. These model calculations, previously validated during the EXPOSE-E and EXPOSE-R missions, were provided by RedShift Design and Engineering (Belgium). For each sample location, the wavelength-dependent irradiance in $W/m^2$ was computed for UVC (100–280 nm), UVB (280–315 nm), and UVA (315–400 nm), as well as for the full spectrum over the 100–1000 nm range. Particle radiation detection utilized a passive radiation dosimeter, R3D, positioned adjacent to the upper compartment of the exposure platform (Berger et al., 2016; Rabbow et al., 2012). The temperature profile, contingent on the platform's orientation relative to the Sun, was not directly measured on the sample compartment but was averaged from nine temperature sensors spanning the entire monoblock (Rabbow et al., 2017). In the ground experiment at MUSC, the temperature profile was emulated using a temperature-controlled interface for the sample compartments. The total irradiance was mimicked using a xenon arc lamp-driven solar simulator, which allowed irradiation with an artificial solar spectrum encompassing wavelengths longer than 200 nm. Adjusting the total irradiance necessitated the utilization of a calibrated double monochromator beforehand, with the aim to replicate the total irradiance level in the wavelength range 200–400 nm (Rabbow et al., 2017). In the time-resolved experiment, irradiation was provided by a solar simulator SF-300-A (Sciencetech Inc., Canada), powered by a xenon arc lamp, with the total irradiance calibrated based on *EXPOSE-R2* data. Individual measurements of irradiation at each sample site were conducted using a calibrated UV-Vis spectrometer (HR4000, Ocean Insight, Germany) to account for nonuniformity across the irradiation beam cross-section area. Temperature was recorded via a Pt1000 RTD (resistance temperature device) situated near the sample; however, no active temperature control was administered. At intervals of 10 h, samples were carefully extracted from the mask and analyzed. The radiation and temperature data of both EXPOSE-R2 and the time-resolved experiment are summarized in Supplementary Table S1 in the supplementary information; in short, the UV-light (200–400 nm) dose received by ISS-exposed samples, ground-exposed samples, and laboratory analogs for time-resolved spectroscopy was 739, 658, and 117 $MJ/m^2$, respectively. The ISS-exposed and ISS-dark samples received particle radiation with an overall mission dose of approximately 410 mGy. The temperature fluctuated between 20°C and 50°C in the EXPOSE-R2 experiment and was kept at room temperature for the time-resolved spectroscopy experiment.

### 2.3. Sample species and preparation

Both experiments employed three distinct sample configurations to analyze the impact of radiation on alanine within three specific scenarios that could mirror conditions on the martian surface, as visually represented in Fig. 2: a pure alanine thin film, an alanine thin film shielded from UV exposure by a separate layer of montmorillonite, and an alanine-montmorillonite composite layer, wherein alanine is intercalated into the clay's interlayers, forming an organoclay. Alanine ($H_2N$-CH($CH_3$)-COOH) is electrically neutral in the gas phase, while it adopts a zwitterionic configuration in the solid phase, where the protonated amino group ($NH_3^+$) carries a positive charge and the carboxylate group ($COO^-$) is negatively charged. The α-carbon connects these functional groups and is the lone chiral center. Alanine predominantly exists in nature in levorotatory form (L-alanine). Although the origins of homochirality lack a definitive scientific explanation, there is evidence pointing to chiral imbalances even in extraterrestrial samples (Cronin and Pizzarello, 1997). The dextrorotatory form (D-alanine) shares identical chemical characteristics with L-alanine, whereas the racemic form (Rac-alanine) differs in the solid state from the individual enantiomers in their solid states in the orientation of ionic bonding due to its distinct crystal structure (Kamei et al., 2018). Both sample configurations of alanine in connection with montmorillonite clay include the two enantiomers of alanine as well as the racemic form, facilitating the detection of potential deviations in their photokinetics; it has been reported that clay minerals can have stereoselective adsorption properties with chiral organic compounds (Valaskova and Martynkova, 2012), which potentially can impact their photostability in a stereoselective manner. Montmorillonite, classified as a smectite-type clay, adopts a 2:1 layer arrangement that comprises two silica tetrahedral sheets enveloping an octahedral sheet that typically incorporates cations such as $Al^{3+}$, $Mg^{2+}$, or $Fe^{2+}$. These layers have a thickness of around 1 nm and are separated by an interlayer space of 0.3–0.5 nm, capable of housing interlayer cations such as $K^+$, $Na^+$, or $Cs^+$ (Salam and Davies, 2015; Uddin, 2008). Each sample was confined within a high-vacuum sealed stainless steel cylinder, with a Viton O-ring interposed between the cylinder and each of two disc-shaped magnesium fluoride ($MgF_2$) substrates, having an estimated leak rate of approximately $10^{-5}$ mbar·l/s (Bumay and Nelson, 1991). The layers were applied to the inner-facing surface of the $MgF_2$ substrates (diameter = 11 mm, thickness = 1 mm), which possess high transparency across a broad wavelength spectrum range from 120 to 8000 nm (1250 $cm^{-1}$) that allows for both UV irradiation in space and infrared spectroscopy. For the time-resolved spectroscopy experiment, two $MgF_2$ substrates were stacked, separated by a brass ring without further sealing. This design was employed as the sample specimens were continuously kept in a nitrogen-purged glovebox (99.999%) at an oxygen and $H_2O$ level each below 0.1 parts per million (ppm) to minimize any chemical reactions with the environment. The structure of the sample container and the various $MgF_2$ stacks for time-resolved spectroscopy allowed for different orientations of the sample layer relative to the UV radiation source (see Fig. 2d). Within *EXPOSE-R2*, a single sample of Rac-alanine thin film was utilized. In contrast, for the other two sample configurations, all enantiomers and orientations were included, yielding a total of 13 samples (see Fig. 2e). Additionally, a blank $MgF_2$ substrate was included in all sample sets to serve as a control for postflight contamination assessment. The

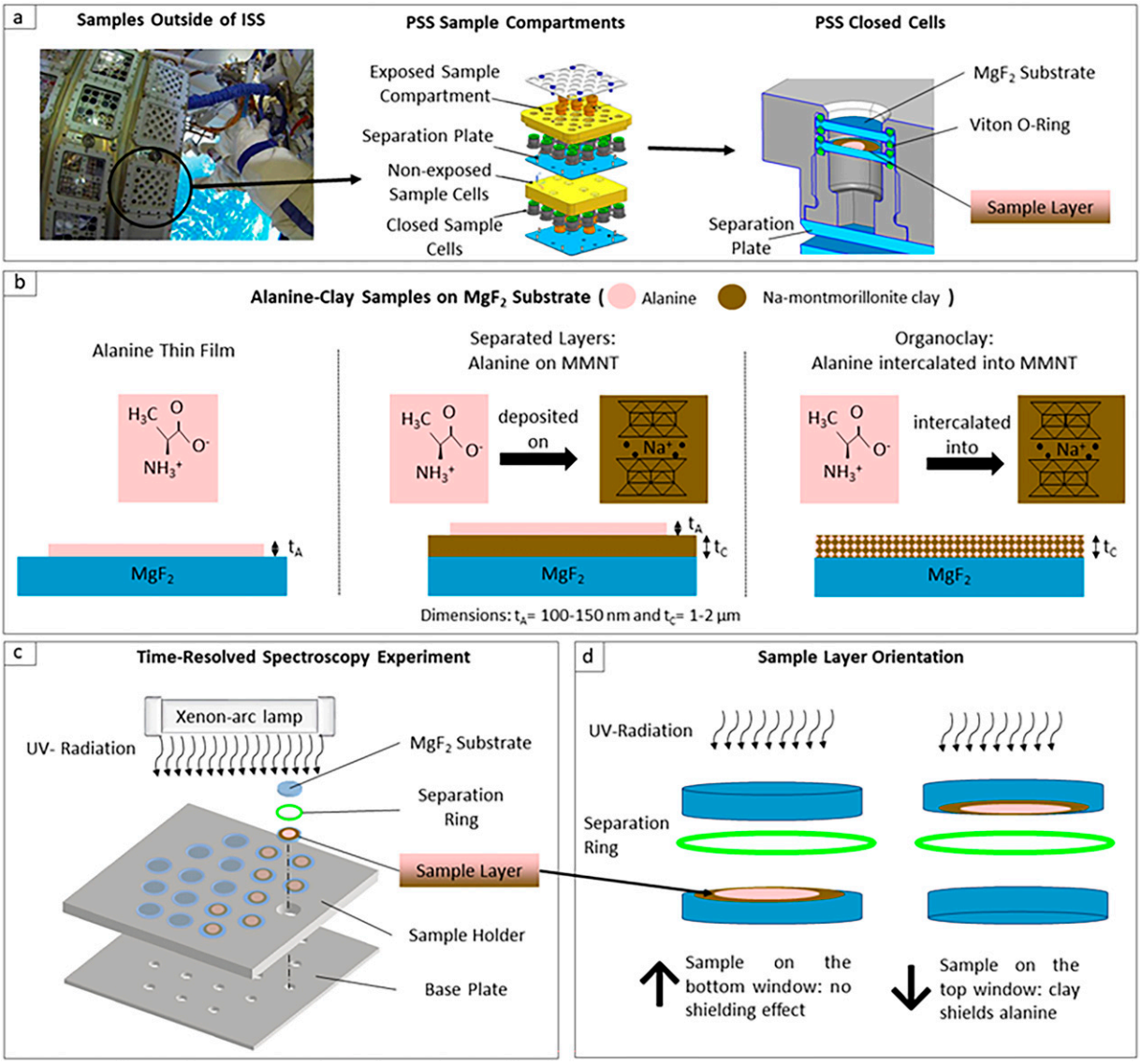


**FIG. 2.** **(a)** Left column: Photograph of the EXPOSE-R2 samples positioned within compartments on a monoblock, situated on the exterior of the ISS (photo credits: ESA, Roscosmos, and DLR). Center column: Exploded view of a sample compartment in the closed-cell configuration, with exposed samples positioned above and dark samples below. Right column: Schematic representation of the O-ring-sealed closed sample cells (11 mm in diameter and 6 mm in height), allowing for different orientations of the sample layers in relation to the incident UV radiation. **(b)** Sample variants placed on transparent $MgF_2$ substrates: solid thin film of zwitterionic alanine (left column), thin film on $Na^+$-montmorillonite layer (center column), and a layer of alanine intercalated into $Na^+$-montmorillonite (organoclay). Montmorillonite clay is denoted with the suffix "MMNT"; dimensions are not to scale but values for the layer thicknesses are given. **(c)** Schematic representation of the sample irradiation setup for the time-resolved spectroscopy experiment, with a xenon-arc lamp-driven solar simulator used as irradiation source. The sample holder allows for 19 sample spots, each comprising two stacked $MgF_2$ substrates (separated by a O-ring), imitating the closed sample cells of the PSS experiment. **(d)** More detailed perspective of sample layer orientations: each sample type comprised two specimens, each oriented differently, to simulate shielding by the clay layer. PSS, Photochemistry on the Space Station.

ensuing time-resolved experiment comprised a single set consisting of 18 samples. This encompassed two additional L- and D-alanine thin films, along with a $MgF_2$ substrate supporting a pure montmorillonite layer, deployed to analyze the clay's photochemical kinetics.

2.3.1. Alanine thin film samples. A $MgF_2$ substrate (purchased from MolTech, Germany) supporting a thin film of Rac-alanine was included in the experiments to validate that alanine's photostability is insufficient for it to survive the total irradiation dose delivered over the full 15.5 months' duration of the space mission. This aligns with laboratory experiments conducted under analogous conditions (ten Kate et al., 2005). In subsequent time-resolved spectroscopy experiments, L- and D-alanine thin films were included, which facilitated the detection of potential deviations in the photokinetics of the two enantiomers. The alanine thin films were prepared via thermal evaporation under high-vacuum

conditions, supplemented by quartz crystal microbalance measurements of thickness via mass loading (alanine with purity >99%, purchased from TCI Chemicals, Japan). This approach allowed for the deposition of thickness-controlled ultra-thin and exceedingly uniform organic films. The thickness of the deposited layer was assessed for each evaporation batch via atomic force microscopy on an additionally prepared sample. The measurements indicated a layer thickness of approximately 150 nm for all amino acid samples deposited onto clay and 100 nm for the samples intended for time-resolved spectroscopy.

2.3.2. Montmorillonite pretreatment. We used a sodium-rich SWY-2 montmorillonite clay, obtained from the Clay Mineral Society (Kogel and Lewis, 2001). The clay underwent a series of procedures before being prepared in thin-film form for experimental specimens. It was initially cleansed with $H_2O_2$ and HCl to remove organics and other cations, yielding an $H^+$-montmorillonite. Subsequently, sodium cations were introduced into the interlayer space between the tetrahedral layers of the clay through a washing process involving NaCl. Ultimately, a purification process involving washing with deionized water and dialysis followed by drying was conducted. The characteristics of the resulting clay including the water content after preparation will be discussed in Section 3.1. The clay preparation steps followed the method described in detail by Banin et al. (Banin et al., 1985).

2.3.3. Alanine on montmorillonite clay-separated layers. A suspension of montmorillonite (1% w/v) was pipetted onto the $MgF_2$ substrates within a controlled clean-air laminar-flow environment, preceding the subsequent deposition of L-, D-, and Rac-alanine thin films. The pipetted volume (50 μL), in combination with the substrate's surface area, resulted in layer thicknesses ranging from 1 to 2 μm after the drying process, exhibiting slight nonuniformities across the layer, as examined by scanning electron microscopy. Subsequently, alanine thin films were deposited as separate layers atop the montmorillonite layer. These alanine-clay composite samples possessed the same alanine thickness as the pure alanine samples. Due to montmorillonite's notably large surface-area-to-mass ratio (>100 $m^2/g$) and its high absorbency for simple organic compounds (Mortland, 1970), alanine becomes chemisorbed at the montmorillonite interface. To assess the stability of alanine when shielded by the clay mineral, two identical samples were prepared for each alanine enantiomer. Each of these samples was oriented with either the alanine or the clay facing the irradiation source.

2.3.4. Alanine intercalated into montmorillonite clay: organoclay. To explore the bulk shielding effects of montmorillonite and its photochemical interaction with alanine, an alanine-montmorillonite organoclay was synthesized. An aqueous solution of excess L-, D-, or Rac-alanine (22 mM) was mixed with a suspension of montmorillonite (1% w/v). After a 48-h period on a rocking table, the solution underwent centrifugation for 20 min at a rotation speed of 2500 $min^{-1}$, followed by removal of supernatant water using a pipette. An additional washing step with purified and deionized water was employed to remove excess alanine. Ultimately, the resulting suspension (V = 50 μL) was pipetted onto the $MgF_2$ substrates and subsequently dried in a laminar-flow environment. Following the drying process, the organoclay layers exhibited a final thickness ranging from 1 to 2 μm. The quantity and orientation of the organoclay samples mirrored those of the separately layered samples (refer to Fig. 2).

### 2.4. Sample analysis

FTIR spectroscopy was employed in both experiments for sample characterization and *in situ* analysis. Following the preparation and assembly of the sample container, preflight spectra were acquired at a spectral resolution of 0.5 $cm^{-1}$ using an Excalibur FTS-4000 FTIR spectrometer (Bio-Rad Laboratories Inc., USA) purged with dry air. Samples returned from the ISS, as well as ground-control samples, were analyzed postflight with a spectral resolution of 1 $cm^{-1}$ using a Tensor 27 FTIR spectrometer (Bruker Optics Ltd., UK) purged with nitrogen. For the time-resolved measurements, a miniaturized FTIR spectrometer with a spectral resolution of 4 $cm^{-1}$ was utilized (FTIR-OEM, Arcoptix Switzerland).

### 2.5. Sample characterization

All samples were analyzed using FTIR spectroscopy with a specific focus on the alanine fingerprint region from 1750 to 1280 $cm^{-1}$. These data were subsequently processed with a statistics-sensitive nonlinear iterative peak-clipping baseline-correction method (Ryan et al., 1988). For the investigation of the photokinetic decay of alanine, each infrared band was assigned to the corresponding vibrational mode of the molecule, thus identifying the bonds involved. Alanine degradation kinetics were fit to a first-order exponential process (Ehrenfreund et al., 2001; Johnson et al., 2012). After time $t$ under electromagnetic irradiation, the number of remaining intact molecules, $m(t)$, can be related to the change in number of intact molecules as follows:

$$\mathrm{d}m(t) = -m(t)\int \sigma(\nu)I(\nu)\Phi(\nu)\,\mathrm{d}\nu\,\mathrm{d}t \tag{1}$$

where $\sigma(\nu)$ signifies the molecular absorption cross section, $I(\nu)$ represents the radiation intensity, and $\Phi(\nu)$ is the quantum yield of the photolytic reaction, with all three values depending on the wavelength, $\nu$. The molecular decay rate is

$$J = \int \sigma(\nu)I(\nu)\Phi(\nu)\,\mathrm{d}\nu \tag{2}$$

Similarly, the molecular bond-specific decay rate $J_b$ can be calculated with $\sigma_b$ and $\Phi_b$ the respective bond-specific absorption cross-section and photolytic quantum yield:

$$J_b = \int \sigma_b(\nu)I(\nu)\Phi_b(\nu)\,\mathrm{d}\nu \tag{3}$$

The bond-specific absorption, in relation to the bond-specific decay rate, can then be represented as

$$A_b(v,t) = A_{0,b}(v)e^{-J_b t} + A(v)_{End,b} \quad (4)$$

where $A_{0,b}(v)$ is the initial bond-specific absorption and $A(v)_{End,b}$ accounts for any residual absorption (e.g., due to decomposition products) once all the original molecules are gone. Consequently, the half-life, $\tau_H = \ln(2)J_b^{-1}$, for the respective bond can be deduced from the time dependence of the absorption spectrum. For each bond-specific absorption peak, we computed the integral using an individual integration baseline.

## 3. Results

The bond-specific infrared absorption bands enable us to examine the photo-induced degradation kinetics of alanine's individual chemical bonds. Our findings also permit a comparison of the photostability of alanine as a pure thin film and in contact with or mixed with montmorillonite clay. While all UV-exposed samples sent to space-exhibited complete degradation postflight, time-resolved spectroscopy effectively elucidated the photo-decay dynamics inherent to each sample configuration. Our observations reveal that clay layers measuring a few micrometers did not provide effective UV shielding. However, time-resolved measurements and postexposure examination reveal that liberated $CO_2$ trapped within the organoclay can be distinctively identified as a photolytic byproduct that results from the alanine decay.

### 3.1. Infrared spectra absorption peak assignment

The acquired infrared spectra subsequent to thermal evaporation indicated that the alanine thin films were deposited as a mixture of neutral and zwitterionic forms. However, exposure to the atmosphere led to the prevalence of the zwitterionic state. This phenomenon is triggered by atmospheric $H_2O$ (Bowles et al., 2022; Rodríguez-Lazcano et al., 2012) and can also be observed with another amino acid, glycine (Mate et al., 2011). Spectroscopic analysis (refer to appendix, Supplementary Fig. S1) unveiled that this transition occurs within a few seconds in a standard air atmosphere at approximately 45% relative humidity. Nevertheless, the mixed form endured within the alanine thin films for months when stored in a dry nitrogen atmosphere. Considering that the *EXPOSE-R2* sample exposure started approximately 3 months after their preparation and factoring in the estimated leak rate ($10^{-5}$ mbar·l/s, Section 2.3) of the closed cell configuration, we expect the alanine films to have been largely in the zwitterionic form at the onset of irradiation. Consequently, we devised a spectroscopic transfer function for each sample species, leveraging preflight and postflight spectra from the respective sample specimen of the reference sample set (dark, T = 5°C). This enabled us to compute the absorption spectrum in the zwitterionic form for each sample at the onset of the experiment. Notably, samples intended for time-resolved measurements were exposed to air for 5 min immediately after the evaporation and therefore did not require recalculation.

Illustrated in Fig. 3a, the transfer function was applied for the ISS dark Rac-alanine thin film sample. Fig. 3b,c, and d depicts the recalculated preflight spectra for each of the three sample configurations, along with the respective peak assignment in the alanine fingerprint region. In Table 1, we associate each absorption band with the related chemical bond. These peak assignments were determined by comparing multiple studies, which presented slightly different interpretations. (Bowles et al., 2022; Cao and Fischer, 2000; Caroline et al., 2009; Garcia et al., 2008; Minkov et al., 2010; Mohamed and Mohammed, 2013; Rodríguez-Lazcano et al., 2012; Rosado et al., 1997; Rozenberg et al., 2003; see Supplementary Table S2 for a full comparison of nonunivocal peak assignments in the literature). For some peak assignments, discrepancies can be attributed to band overlap and mode mixing (Garcia et al., 2008). The bands centered at 1356 and 1412 $cm^{-1}$ are ascribed to $\nu_S COO^-$ or $\delta_{as}CH_3$, whereas the 1307 $cm^{-1}$ band corresponds to $\delta$CH or $\delta NH_3^+$. The features centered around 1589 and 1623 $cm^{-1}$ are linked to the $COO^-$ group or $\delta NH_3^+$. However, the literature is not clear on this point, and it is possible that mode mixing contributes to the differing peak assignments and discrepancies observed in studies. The L-alanine and D-alanine thin films possess identical absorption spectra, although the intensity of the $\delta NH_3^+$ bands varies. The presence of the mineral clay alters the infrared spectrum of alanine; this indicates chemisorption of alanine and clay. In the case of samples that featured separated layers (as shown in Fig. 3c), the band associated with $\nu_S COO^-/\delta_{as}CH_3$ at 1412 $cm^{-1}$ coincides with a $\delta$NH mode of the clay. In fact, during solvent casting, ammonium ions can form and bind to montmorillonite, giving rise to an absorption feature at 1425 $cm^{-1}$ (Kozak and Domka, 2004; Mortland et al., 1963; Russell, 1965). The interaction between clay and alanine also gives rise to a $\delta_s COO^-$ band at about 1380 $cm^{-1}$ and a C=O stretch of the alanine carboxylic group at 1720 $cm^{-1}$ (Bu et al., 2019; Jang and Condrare, 1972). The interaction processes between clay and alanine described above are naturally stronger in the organoclay samples, leading to a further broadening of the band at 1602 $cm^{-1}$. This broadening arises from the superposition of the $\nu_S COO^-$, $\nu_{aS}NH3^+$ (from the alanine), and the montmorillonite structural $\delta$OH bond. The latter further results, upon superposition with the $\nu_S COO^-/\delta NH_3^+$ absorption, in a combined band at 1620 $cm^{-1}$. This band becomes more pronounced when the clay contains bound $H_2O$, due to superposition with the $\delta$OH vibration of the $H_2O$ (Kuligiewicz et al., 2015). In this context, the hydration state of montmorillonite can be estimated by a characteristic band at around 3400 $cm^{-1}$, assigned to a $\delta$OH vibration of water (Kuligiewicz et al., 2015; Venyaminov and Prendergast, 1997; Yeşilbaş et al., 2018). As illustrated in Supplementary Fig. S2, we observed a slight increase of absorption at around 3400 $cm^{-1}$ in all *EXPOSE-R2* samples, whereas no absorption band could be identified for the samples for time-resolved spectroscopy, implying higher water content in the clay prepared for *EXPOSE-R2* samples. The shoulder observed at around 1500 $cm^{-1}$ emerges from interactions between the $\delta$OH and the $NH_3^+$ groups, indicating adsorption processes at the interface of the alanine thin film and separated clay layers (Bertie and Morrison, 1980; Friebele et al., 1980; Max and Chapados, 2013; Zheng et al., 2009).

### 3.2. Alanine thin film stability

Both the ISS-exposed and ground-exposed Rac-alanine thin film samples exhibited complete degradation postflight, as indicated by the absence of any recognizable alanine-

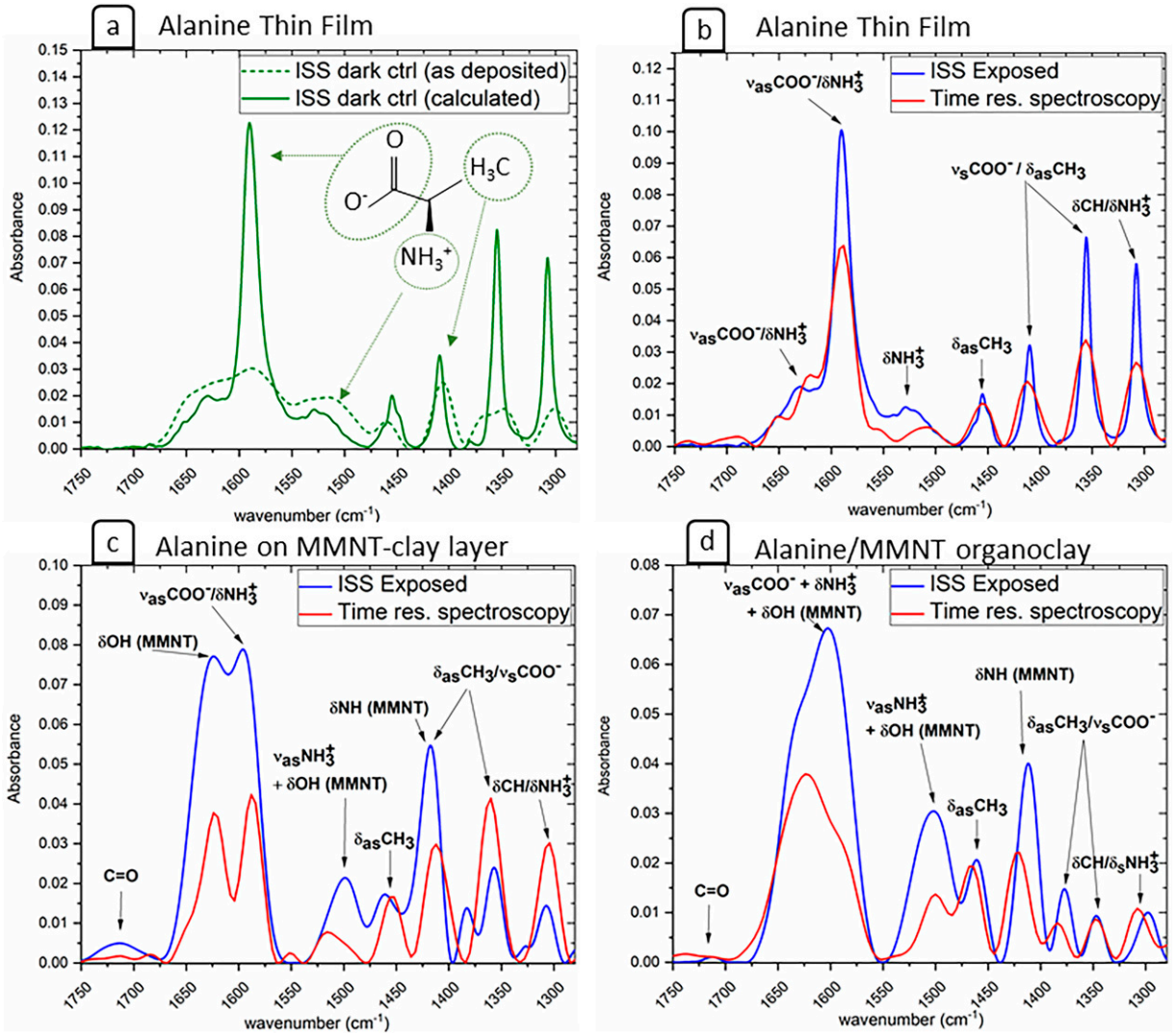


**FIG. 3.** **(a)** For all amino acid–clay samples, the infrared spectra of zwitterionic alanine at the start of the experiment were calculated based on the infrared spectra acquired immediately after thin film deposition (demonstrated using the spectra of the ISS dark Rac-alanine sample). The specific chemical groups constituting the (zwitterionic) alanine structure, all connected via the central α-carbon, can be correlated with distinct infrared absorption bands. **(b–d)** Display the infrared spectra of the three sample configurations at the initiation of the experiments, for both the ISS-exposed and time-resolved spectroscopy samples in each case. Specifically, **(b)** shows Rac-alanine thin films, **(c)** shows a D-alanine thin film on a separate montmorillonite layer, and **(d)** portrays L-alanine/montmorillonite organoclay. Montmorillonite clay is denoted with the suffix "MMNT."

related features in their spectra. The time-resolved spectroscopy measurements captured the photokinetic decay of the individual bands of Rac-alanine, illustrated in Fig. 4. The calculated half-lives for all enantiomers, ranging from 60 to 76 h, are summarized in Fig. 4, right-hand side. The absence of intrasample shielding by upper thin film layers, which would have led to an altered exponential degradation curve (Baratta et al., 2019), suggests a uniform photodegradation process across the depth of the thin film layer. All calculated half-lives were derived from normalized integrals of the chemical bond absorbance for each measurement and thereby captured the time evolution of the respective bond absorption. Employing Eq. 4, an exponential fit was used under the assumption of absorption convergence to zero, and the parameter $A(v)_{End,b}$, along with the deviation of each peak from an ideal Gaussian curve, was utilized for error determination. Due to the low intensity of the $\delta_{as}NH_3^+$ band at 1525 $cm^{-1}$, which resulted in a substantial integration error, it was excluded from the analysis. In the case of Rac-alanine, the bands at 1589 and 1626 $cm^{-1}$ overlapped and thus were treated as a collective band for integration. Importantly, it should be noted that the different samples received varying radiation doses, and the intensity $I_\Phi$ was calculated based on the measured total irradiance provided by the solar simulator at the respective sample location.

### *3.3. Photostability of alanine thin film on montmorillonite layer*

All UV-irradiated (ISS-exposed and ground-exposed) samples exhibited complete degradation postflight, except for the two montmorillonite peaks, as illustrated in Fig. 5.

TABLE 1. ASSIGNMENT OF DISTINCT ABSORPTION BANDS OBSERVED IN THE INFRARED SPECTRA OF THE VARIOUS SAMPLE SPECIES (AND SUBSEQUENT LABORATORY SIMULATION)

| | *Band peak position* $\overline{\nu}(cm^{-1})$ | | |
|---|---|---|---|
| | *Alanine* | *Alanine/MMNT* | |
| *Vibrational mode* | *Film* | *Layer* | *Organoclay* |
| $\delta CH$ / $\delta NH_3^+$ | 1307 | 1307 | 1300 |
| $\nu_S COO^-/\delta_{as} CH_3$ | 1356 | 1356 | 1346 |
| $\delta_s COO^-$ | — | (1382) | 1376 |
| $\nu_S COO^-/\delta_{as} CH_3$ | 1412 | 1415 (+$\delta$NH) | 1415 (+$\delta$NH) |
| $\delta_{as} CH_3$ | 1456 | 1457 | 1460 |
| $\delta_{as} NH_3^+$ | 1512, 1525 | 1500 (+ $\delta$OH) | 1500 (+ $\delta$OH) |
| $\nu_S COO^-/\ \delta_{as} NH_3^+$ | 1589 | 1594 | 1602 (+ $\delta$OH) |
| $\nu_S COO^-/\ \delta_{as} NH_3^+$ | 1626 | 1620 (+ $\delta$OH) | 1602 (+ $\delta$OH) |
| $\nu$C=O | — | 1720 | 1720 |

The assignment of absorption bands is in accordance with available literature, although certain bands have inconsistent assignments across sources (Bowles et al., 2022; Cao and Fischer, 2000; Caroline et al., 2009; Garcia et al., 2008; Minkov et al., 2010; Mohamed and Mohammed, 2013; Rodríguez-Lazcano et al., 2012; Rosado et al., 1997; Rozenberg et al., 2003). Greek letters denote the type of vibration ($\nu$ for stretching and $\delta$ for bending), while subscripts denote the symmetry type of the vibration ("s" for symmetric and "as" for antisymmetric). Montmorillonite clay is denoted with the suffix "MMNT".



Notably, a $\delta$NH peak shift from 1416 to 1425 $cm^{-1}$, attributed to alanine bond decay, is observable. Interestingly, a significant UV shielding effect by the clay was observed through time-resolved spectroscopy. This shielding effect leads to an increase in alanine stability of about an order of magnitude, as shown in Table 2. Conversely, unshielded samples displayed an inverse process; the half-lives of alanine thin films on montmorillonite, without shielding, were reduced compared with the thin film samples without a clay layer across all instances. Prior to calculating the half-lives, the corresponding spectrum of the montmorillonite sample was subtracted for each time point to eliminate any bias due to radiation-induced changes in the clay itself. Among the irradiated samples, we observed a slight increase in absorbance around 2345 $cm^{-1}$, which indicated the presence of gaseous $CO_2$ in the clay interlayers. This phenomenon, however, was considerably more pronounced in the irradiated organoclay samples and will be described in more detail in the subsequent section.

### 3.4. Photochemistry of Na-montmorillonite organoclay

The irradiated organoclay layers exhibited no traces of alanine; only montmorillonite was detectable in the fingerprint region. Through the time-resolved measurements, it was discovered that their half-lives on average were slightly

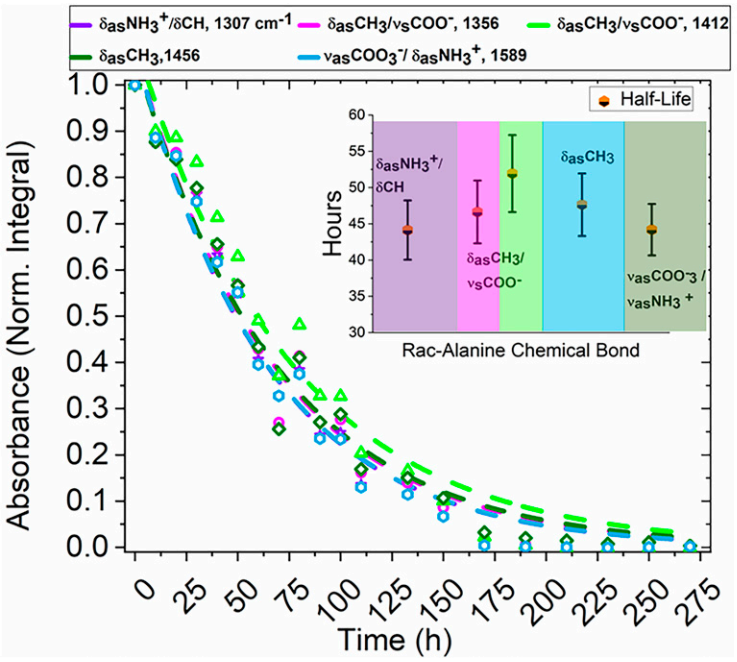


**Alanine Thin Films: Half-Life Times (Averaged from ↑- and ↓- Sample)**

| Absorption Band ($cm^{-1}$) | Rac-Ala (↑↓) | L-Ala (↑↓) | D-Ala (↑↓) |
|---|---|---|---|
| 1307 | 64 ± 4 h | 61 ± 4 h | 63 ± 6 h |
| 1356 | 67 ± 4 h | 64 ± 4 h | 65 ± 6 h |
| 1412 | 76 ± 5 h | 69 ± 5 h | 70 ± 6 h |
| 1456 | 69 ± 4 h | 66 ± 4 h | 66 ± 6 h |
| 1589 | No Band | 60 ± 9 h | 60 ± 7 h |
| 1589+1620 overlap | 64 ± 6 h | No Band | No Band |
| 1620 | No Band | 64 ± 4 h | 65 ± 7 h |

**FIG. 4.** Left column: Normalized photokinetic UV degradation, expressed as absorbance versus time, and corresponding half-lives of Rac-alanine chemical bonds (inset, for 100 nm thin film), derived from integrated band absorption of each respective feature. Right column: Half-lives of individual chemical bonds of Rac-, D-, and L-alanine thin film samples calculated from averaging the half-lives of both sample orientations.

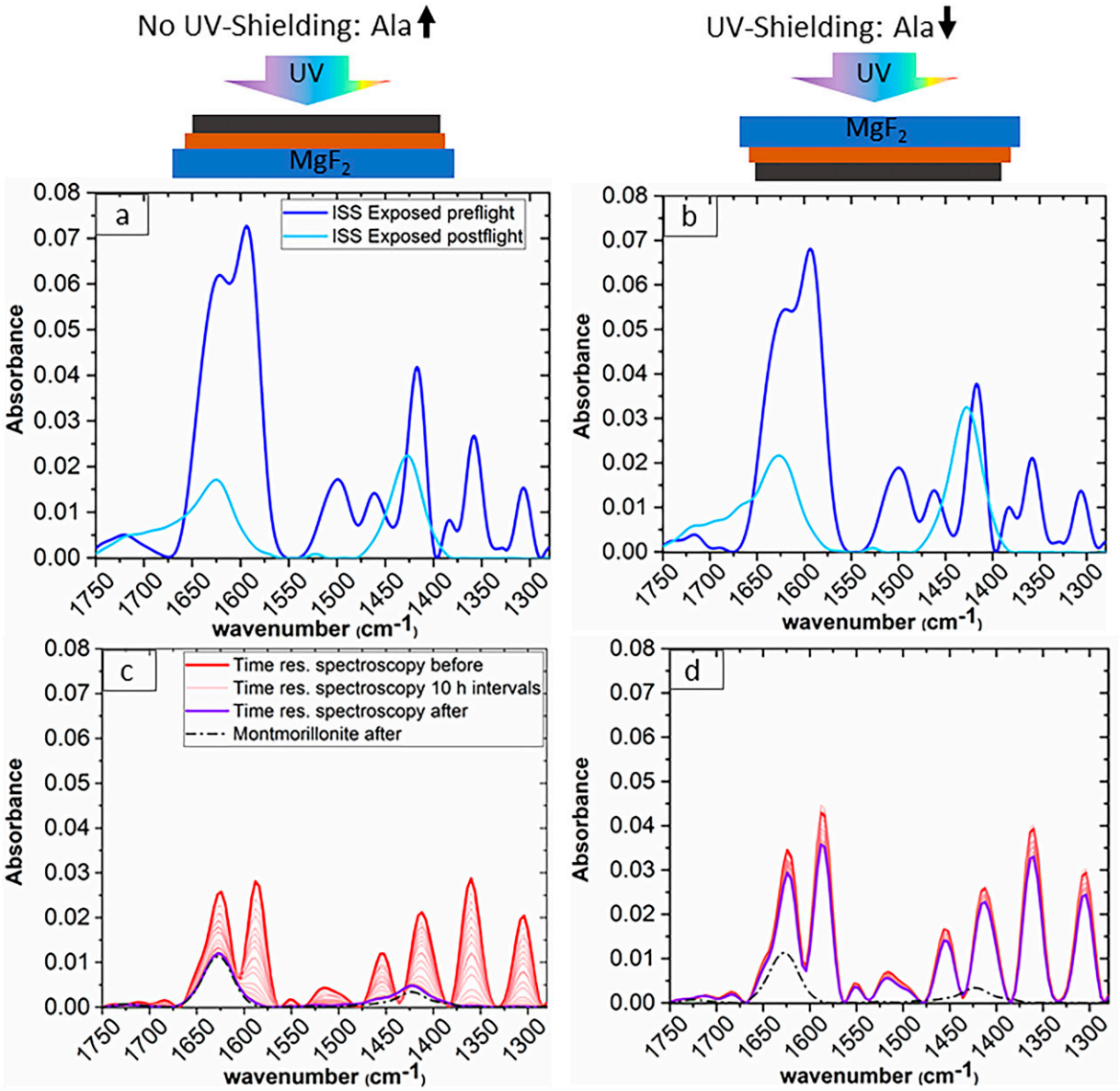


**FIG. 5.** Spectra of irradiated L-alanine thin film on montmorillonite layer with alanine on top of the clay (left column) and beneath the clay (right column) in relation to the irradiation source, as illustrated in the schematic on the top. The alanine in the ISS-exposed samples **(a** and **b)** and the unshielded alanine in the time-resolved spectra **(c)** are entirely degraded. However, time-resolved spectroscopy reveals a significant shielding effect due to the presence of the clay **(d)**. The thin lines in the time-resolved spectra depict spectra during irradiation. The spectrum of the pure clay layer after irradiation (represented with a black dotted line) is included in the spectra of time-resolved spectroscopy for comparison.

extended compared with the pure thin films. The band at 1412 $cm^{-1}$ was not subjected to analysis due to an overlap by the strong and photochemically stable $\delta$NH band of montmorillonite. The $\delta_s COO^-$ band at 1380 $cm^{-1}$ decayed prior to the first measurement (hence it has a half-life of <10 h), and the two alanine bands at 1589 and 1625 $cm^{-1}$ were

Table 2. Averaged Half-Lives of Alanine Thin Films on Montmorillonite Clay

| | *Rac-Ala* ↑[a] | *Rac-Ala* ↓[b] | *L-Ala* ↑ | *L-Ala* ↓ | *D-Ala* ↑ | *D-Ala* ↓ |
|---|---|---|---|---|---|---|
| | $I_\Phi = 1.08$ | $I_\Phi = 0.98$ | $I_\Phi = 1.03$ | $I_\Phi = 1.05$ | $I_\Phi = 0.92$ | $I_\Phi = 0.93$ |
| Half-life (average) | 59 ± 5 h | 1300 ± 800 h | 57 ± 3 h | 1100 ± 180 h | 61 ± 6 h | 1400 ± 1100 h |

[a,b]The arrows in the top row indicate whether the Ala film directly faces the irradiation source (up arrows) or is protected by a layer of clay from the illumination (down arrows). The half-lives have been adjusted according to the relative received irradiation intensity at their specific locations, denoted as $I_\Phi$.

combined in integration. All ISS-exposed organoclay samples were completely degraded postflight, which was confirmed by the organoclay photodegradation profile and the calculated half-lives of all alanine/montmorillonite organoclays obtained through time-resolved spectroscopy, as depicted in Supplementary Fig. S3 (for D-alanine organoclay) and Supplementary Table S3 in the appendix. Within the postflight spectra, the emergence of a peak at about 2345 $cm^{-1}$ was observed in all irradiated samples. This peak can be attributed to the asymmetrical stretching vibration of intercalated gaseous $CO_2$ (Romanov, 2013; Yeşilbaş et al., 2019). The presence of the $CO_2$ band absorption in the D-alanine ISS- and ground-exposed spectra, contrasting with the absence of the $CO_2$ band in the corresponding spectra of the dark samples, is clearly evident in Fig. 6a. To compute the $CO_2$ production rate in the organoclay, the $CO_2$ abundance in the time-resolved spectroscopy samples was utilized (Supplementary Fig. S4 in the appendix). The increase of the $CO_2$ concentration is shown in Fig. 6b, along with the exponential decay of the D-alanine thin film absorption bands at 1589 and 1620 $cm^{-1}$, which are associated with the alanine $COO^-$ bond (discussed in Section 3.1). The $CO_2$ concentration increases rapidly initially, but ever more slowly with time, in all analyzed samples, until there is no alanine left to degrade and the $CO_2$ concentration plateaus, corresponding to absorption $A_s$. Fitting the $CO_2$ absorbance to Eq. 5 provides a good approximation, as Fig. 6b shows:

$$A(t) = A_s(1 - e^{-Gt}) \tag{5}$$

Normalizing to $A_S = 1$ for the limiting amount of evolved $CO_2$, we calculated the growth rate $G$. The half-time $\tau_H$, in which the $CO_2$ concentration reaches half of the maximum absorption, compares well with the bond-specific half-lives and is listed in Supplementary Table S3.

### 3.5. Ground experiment verification

The spectra of the ISS dark and ground dark samples were analyzed and compared to determine degradation effects not attributable to UV radiation and to examine deviations between space and ground samples. The postflight spectra of both samples exhibit reduced absorption compared with their preflight absorption, as shown in Supplementary Fig. S5. Integration over the wavenumber range from 1680 to 1280 $cm^{-1}$ results in an absorption reduction of 5.3 ± 0.7% and 4.5 ± 0.8% for ISS and ground samples, respectively.

### 3.6. Window contamination

While the presence of organic contaminants on the outside of the sample compartments does not pose a direct threat to samples, it can diminish the windows' transmittivity through photofixation under solar irradiation, resulting in changes of the received irradiation doses that are difficult to trace without *in situ* monitoring. To control for contamination in our samples, we conducted postflight UV-transmission measurements on the blank $MgF_2$ windows at the ASTRID2 synchrotron radiation facility at Aarhus University, Denmark, within the wavelength range of 125–280 nm. A significant reduction in transmittivity was observed on the bottom windows of the irradiated sample compartments as shown in Supplementary Fig. S6, caused by outgassing of the monoblock (Rabbow et al., 2017). However, this reduction did not impact any of the experimental parameters. Subsequently, we employed atomic force microscopy to examine the contaminated windows. This revealed contamination layers with thicknesses ranging from 20 to 50 nm. The top windows of the irradiated sample compartments exhibited only a slight reduction in transmittivity, which had no effect on the overall findings, as it was considered in the determination of the experimental irradiation doses.

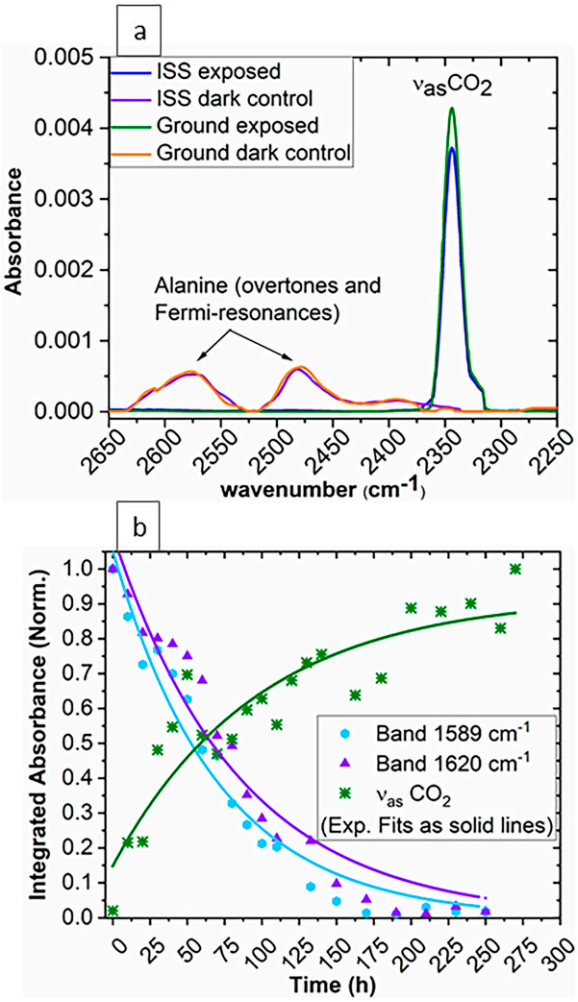


**FIG. 6.** **(a)** Postflight spectra of D-alanine/montmorillonite organoclays: ISS exposed (blue), ground exposed (green), ISS dark (purple), and ground dark (orange). Both unexposed samples exhibit two small peaks attributed to overtones and Fermi resonances of alanine (Garcia et al., 2008), which were not considered for further data analysis. In both exposed samples, the alanine is completely degraded, as indicated by the absence of the alanine peaks. An absorption band of intercalated $CO_2$ at 2345 $cm^{-1}$ arose due to the photochemical interaction of alanine and montmorillonite. **(b)** Illustration of the approach of the $CO_2$ concentration to a constant limiting value in a D-alanine organoclay sample and the approach of the bands at 1589 and 1620 $cm^{-1}$ to zero absorbance for a D-alanine thin film sample. The bands at 1589 and 1620 $cm^{-1}$ are associated with the alanine $COO^-$ bond. All spectra presented here were obtained by time-resolved spectroscopy.

## 4. Discussion

Our experimental results reveal that the capability of montmorillonite to shield alanine from UV radiation is highly dependent on the thickness of the clay layer. Indeed, macroscopic layer thicknesses of millimeters would be required to effectively shield the photochemically unstable alanine over durations of years to millennia. Under certain conditions, the $CO_2$ generated during the photochemical decomposition of the amino acid can remain confined within the clay matrix, which thus suggests its potential use as a marker to provide evidence of past organic compound existence in the martian context.

### 4.1. UV photolysis of enantiomers

The photochemical decomposition of solid alanine thin films can accurately be modeled using an exponential first-order fit (Eq. 4). Two main photolytic pathways of alanine are well-established: decarboxylation (resulting in the loss of the $COO^-$ group with gaseous $CO_2$ as a byproduct) and deamination (leading to the loss of the $NH_3^+$ with ammonia as a byproduct) (Ehrenfreund et al., 2001; Moore et al., 2021; Sagstuen et al., 2004; ten Kate et al., 2005). Alanine has UV-absorption bands at 266 and 200 nm, with the latter displaying particularly strong absorbance. Recent parahydrogen matrix-isolation infrared spectroscopy investigations of alanine have shown that irradiation with both wavelengths yielded the hydrocarboxyl ($HOCO^\bullet$) radical as a direct photoproduct. Subsequent dissociation of the $HOCO^\bullet$ radical releases $CO_2$ and hydrogen as primary photoproducts, with the highest ratio and fastest rate of concentration increase (Moore et al., 2021). Our data suggest that the absorption band at 1589 $cm^{-1}$ is associated with the $COO^-$ bond, as this band exhibits the shortest half-life in L- and D-alanine. However, we cannot fully exclude the possibility that there are also contributions from the $NH_3^+$ bond, as the differences in the half-lives of the bands at 1589 and 1620 $cm^{-1}$ are not sufficiently significant (see Fig. 4, right-hand side). The photochemical stability of the L- and D-enantiomers does not differ significantly from one another, which is consistent with previous studies (Modica et al., 2014). Our findings suggest that the half-life of alanine is below 80 h, which implies that it is incapable of persisting unprotected on the martian surface and in other extraterrestrial environments over geological timescales. In concordance with our results, other experiments have found the half-life of alanine (thin film, 330 nm thick) to be approximately 80 h and the half-lives of two other proteinogenic amino acids, glycine and serine (thin films, some hundred(s) of nm thick), to be 50–80 h, under irradiation at room temperature with irradiation sources mimicking the UV radiation level on the martian surface (Bertrand et al., 2012; ten Kate et al., 2005).

### 4.2. Effects of Na-montmorillonite on alanine stability: UV shielding, photocatalysis, and humidity

Clays are known to effectively absorb UVA and UVB radiation (Brack, 2013; Hassler et al., 2014). However, recent studies have shown that high-energy UVC radiation can penetrate minerals to depths greater than hundreds of micrometers (Carrier et al., 2019). Our results demonstrated that the half-life of all chemical bonds of alanine in the clay-shielded samples increased by about an order of magnitude relative to unshielded samples. In the wavelength range 200–400 nm, the radiation dose calculated for the time-resolved spectroscopy experiment (117 $MJ/m^2$, $t = 270$ h) is about six times lower than for *EXPOSE-R2* (739 $MJ/m^2$). Assuming a comparable total irradiance, $I_{irr}$, this corresponds to an equivalent of about $t = 1705$ h for the *EXPOSE-R2* irradiation period and suggests that, based on the calculated half-lives in Table 2, 25–50% of the preflight alanine should have been present in the ISS-exposed and ground-exposed samples. However, both ISS- and ground-exposed samples were completely UV-degraded, even though a degradation of at most 6% could have been expected due to non-UV-induced degradation processes, as previously outlined in Section 3.5. For the ISS-exposed samples, this result can be attributed to the additional dose of UVC radiation with wavelengths shorter than 200 nm. However, the simultaneous degradation of the ground-exposed samples indicates that the elevated water content in the *EXPOSE-R2* montmorillonite clay (as described in Section 3.1) has a degradative effect on the alanine molecules, which is in accordance with existing literature (Kopacz et al., 2023). Concurrently, the leak rate of the *EXPOSE-R2* sample container allowed for additional atmospheric humidity in the sample layer headspace gas (during storage and transport), whereas the samples for time-resolved spectroscopy were kept within a nitrogen atmosphere ($p_{H2O} < 0.1$ ppm by volume) before and during the experiment. Recent studies found that humidity can have an amplifying impact on the UV photodegradation of organic compounds; this suggests the interaction of organic molecules with excited-state OH• to initiate photochemical reactions (Kopacz et al., 2023; Mattioda et al., 2012), which has been confirmed for the three proteinogenic amino acids tryptophan, glycine, and proline (Liu and Kounaves, 2021).

Moreover, reliable comparisons of ISS- and ground-control experiments with the subsequent laboratory simulation are hindered by the large errors of the calculated half-lives, particularly for D-alanine. This mathematical error is caused by the greatly increased bond stability. The increased bond stability caused bond degradation to still occur within the initial nearly linear-with-time range of the decay. Nevertheless, the experimental data show that montmorillonite clay layers of a few microns thickness do not provide sufficient shielding from UV radiation over long timescales. An estimation based on the Beer–Lambert law, assuming a uniform mineral density and linear light attenuation, suggests that a clay layer thickness of millimeters is required to extend the organic half-lives to approximately $10^5$ years. Taking Mars as an example, organic matter is considered to be effectively shielded from harmful photon radiation at a depth of several micrometers to millimeters and from particle radiation below a depth of several centimeters to meters beneath the surface, depending on the duration in question (Hassler et al., 2014; Mancinelli and Klovstad, 2000; Marschall et al., 2012; Moores et al., 2007; Parnell et al., 2007).

The UV absorption of montmorillonite is primarily attributed to the d-orbital electrons of iron (II) in the mineral (Gauger et al., 2015). Furthermore, the iron can also catalyze reactions that lead to increased decay rates of amino acids (dos Santos et al., 2016; Liu and Kounaves, 2021; Martin, 1980). We observed this effect in the unshielded alanine thin

films deposited on montmorillonite and directly exposed to UV (Fig. 5, panel b). Due to the adsorption of alanine onto the montmorillonite surface at the interface, the presence of the mineral clay accelerates the photochemical decay, as indicated by lower half-lives in comparison to alanine thin films on $MgF_2$ substrates alone. It may be the case that this effect interferes with the aforementioned degenerative effect of bound $H_2O$ in the montmorillonite, which would lead to two simultaneous degradation effects. Based on the molar absorptivity of $H_2O$ (at 3400 $cm^{-1}$), we calculated a weight percent (wt.%) of <5 wt.% water in the clay for the *EXPOSE-R2* samples, which is consistent with infrared spectroscopy studies of montmorillonite clay at different hydration states (Frinak et al., 2005; Nazdracheva et al., 2022). It is noteworthy that the hydration state of the *EXPOSE-R2* samples' montmorillonite clay is comparable with geological conditions as found on the martian surface and subsurface (Wernicke and Jakosky, 2021).

Considering that the photocatalytic effect must also be present for the organoclay samples, our time-resolved measurements reveal that this photocatalysis is accompanied by a shielding effect in the organoclay samples as well. Thanks to the favorable ratio of large surface area to small pore dimensions, montmorillonite can provide effective bulk protection against UV radiation. Previous experiments conducted with alanine concentrations in the μM range have also shown that the preservative effect increases significantly with a higher concentration of intercalated alanine (dos Santos et al., 2016). In our experiments, we used an alanine-saturated organoclay, suggesting that we investigated an organoclay with the highest possible preservation effect in the given configuration. While alanine was not detectable in the ISS- and ground-exposed samples, results from time-resolved spectroscopy during photodegradation showed strong variations in the stability of the individual samples but consistency in the individual bonds of each sample, with the bond at 1356 $cm^{-1}$ being the most stable in each case. The experimental uncertainty of these data prevents us from making definitive statements about stereoselective influences of montmorillonite on alanine. However, we find no strong evidence for such effects. Based on the half-lives of all other bonds compared with the pure thin-film samples, we conclude that the catalytic effect approximately balances the shielding effect for montmorillonite layer thicknesses of a few micrometers.

### 4.3. Photolytic byproduct as possible markers

We observed the formation of $CO_2$, a byproduct of alanine photodecay, trapped within the montmorillonite mineral matrix. This occurrence was exclusive to the irradiated organoclay. Time-resolved spectroscopy showed that the concentration of entrapped $CO_2$ reached a saturation level, as depicted in Fig. 6b. The $CO_2$ formation half-times, at which half of the saturation level is reached, are remarkably similar to the half-lives of the alanine absorption bands at 1589 and 1620 $cm^{-1}$, both associated with the alanine $COO^-$ bond. This suggests that the saturation is primarily caused by finite photochemical decay rather than being a result of the clay's saturated sorption capacity. Using the Beer–Lambert law, we can estimate the concentration of alanine before irradiation and of $CO_2$ after irradiation in the organoclay by considering their respective wavelength-dependent molar absorptivities and the absorption path length. For a 2 μm-thick organoclay layer, we calculated an initial alanine concentration of $9.9 \times 10^{-4}$ $mol/mm^3$ and a maximum $CO_2$ concentration of $9.5 \times 10^{-5}$ $mol/mm^3$, which corresponds to about 10% of the alanine concentration before irradiation. However, this estimate used a simplified approach, as the molar absorptivity of alanine and $CO_2$ is available in the literature for the case of a free gas, neglecting any interaction with an organoclay matrix (Iglesias-Groth and Cataldo, 2022; Kochanov et al., 2016). The degree to which $CO_2$ can be entrapped within the interlayers of montmorillonite is significantly influenced by temperature and the interlayer cation species (Azzouz et al., 2013; Busch et al., 2016; Romanov, 2013). Michels et al. discovered that the $CO_2$ desorption in $Na^+$-smectites begins at $T > -15°C$, while Romanov et al. reported $CO_2$-retention in montmorillonite for a duration of 8 months under ambient conditions (Michels et al., 2015; Romanov, 2013). We observed a temperature dependence that led to $CO_2$ desorption in all organoclay samples prior to postflight measurements. This resulted in $CO_2$ absorption bands approximately an order of magnitude lower than those in the replica samples for time-resolved spectroscopy, which were maintained at room temperature (Supplementary Fig. S4, appendix). However, due to insufficient gas enclosure in both experimental setups, the precise $CO_2$ desorption rate in our study could not be determined.

Irreversible $CO_2$ confinement could potentially signify the past presence of organic compounds, as it is assumed that smectites with small interlayer ion species, such as sodium, generally do not absorb $CO_2$ into the clay interlayers from the environment. Mendel et al. found that sodium-rich montmorillonite clay does not significantly sorb $CO_2$ at an ambient temperature of −20°C and at pressures as high as 15–17 mbar. Although current studies have primarily focused on a limited range of interlayer cation species under specific pressure and temperature conditions, it is clear that the $CO_2$ sorption capacity increases with higher pressure and lower temperature (Mendel et al., 2021). A concurrent formation (and potential enclosure in the montmorillonite interlayers) of ammonia as a photochemical byproduct, arising from alanine deamination (Section 4.1), could not be observed in the postflight spectrum and time-resolved spectroscopy. The corresponding infrared bands of gaseous ammonia are located at around 1630 and 3400 $cm^{-1}$ (Wang and Agmon, 2016), but they are concealed by the strong and photochemically stable $\delta$OH bands of the montmorillonite clay (as described in Section 3.1).

In light of our experimental findings, we conclude that $Na^+$-montmorillonite clay is a highly interesting geological material for astrobiological research. Considering that decarboxylation is a possible photolytic pathway not only for alanine but also for various organic compounds (Hill et al., 1985; Oró and Holzer, 1979), this type of clay mineral might be of broader interest beyond the specific case of alanine organoclays. Given the abundance of montmorillonite clay on the martian surface, this mineral is particularly intriguing for research in this context. However, it remains uncertain whether or not $CO_2$ could be entrapped over geological timescales in these types of clays and thus be a suitable indicator of the past presence of organic molecules.

### 4.4. Non-UV-induced degradation processes

Both the space and the ground nonexposed samples (dark samples) exhibited a decrease in intensity of their vibrational mode bands over time. This phenomenon can be attributed to temperature- and humidity-induced degradation processes. Complementary analyses (Supplementary Fig. S7) confirmed a slight temperature-induced degradation of alanine when exposed to conditions of 60°C and a pressure of 1 mbar at a relative humidity of about 20% for a time period of several days, similar to the total duration of elevated temperatures on *EXPOSE-R2* (Rabbow et al., 2017). Furthermore, the iron contained in the clay can potentially have a non-UV-induced catalytic effect, which was reported for the interaction of organic compounds with metal surfaces (Cruz-Diaz et al., 2020). However, it is challenging to precisely quantify the extent of temperature-induced degradation within our experimental setup. The effects of particle radiation are considered negligible during the experimental period due to the very small interaction cross-section between energetic charged particles and the molecular orbitals of amino acids. In fact, the irradiation by energetic charged particles would require significantly longer timescales to produce substantial alterations in amino acids—timescales that are not compatible with the exposure duration of our samples (Maté et al., 2015; Pilling et al., 2014). In the specific context of *EXPOSE-R2*, Baratta et al. (Baratta et al., 2019) calculated that the energy dose delivered by photons with wavelengths below 200 nm is up to 10 orders of magnitude higher than the energy dose delivered by galactic cosmic rays, South Atlantic Anomaly protons, and Outer Radiation Belt electrons.

## 5. Conclusions

With *EXPOSE-R2*, potential astrobiologically relevant organic compounds were successfully taken to space, exposed to LEO conditions including full-spectrum solar illumination, and subsequently returned to Earth for postflight analysis. A supplementary experiment with replicated samples and the possibility of time-series measurement provided essential data for a thorough understanding of the photochemical processes of amino acids in association with clay minerals. These experiments collectively confirm that the proteinogenic amino acid alanine is inherently unstable under conditions commonly found in currently accessible extraterrestrial environments with significant solar radiation exposure, such as the surface or near-surface regions of Mars. Nevertheless, the interaction between alanine and montmorillonite clay introduces intriguing possibilities for organic-detection strategies. While montmorillonite's catalytic properties and interlayer-bound $H_2O$ accelerate the photochemical decomposition of alanine, it also exhibits the capacity to shield against high-energy UV radiation. However, this protective effect necessitates significant layer thicknesses up to millimeters in order to extend the lifetime of alanine to timescales of hundreds of thousands of years. Our experimental findings suggest that a stereoselective influence of the Na-montmorillonite clay on the photostability of alanine is, if present, beyond the detection limit of FTIR spectroscopy and would need further dedicated detection methods. Notably, montmorillonite with small interlayer ions, particularly sodium-rich montmorillonite, becomes interesting even at shallower depths due to its capability to encapsulate $CO_2$ within its interlayers. $CO_2$, commonly generated during the photolytic degradation of not only alanine but also other organic compounds, holds potential for life detection in a planetary atmosphere as well as on its surface and in its subsurface. Montmorillonite with small interlayer ions does not readily sorb $CO_2$ from the surrounding atmosphere into the interlayers, which makes it a candidate for entrapping $CO_2$ derived from the degradation of organic material. This concept gains significance in extraterrestrial environments, particularly on Mars, where the abundance of this clay type is notable. However, a comprehensive understanding hinges on a thorough knowledge of how historical and current climatic conditions affect the geology of the respective environment, with the aim of excluding the possibility of external $CO_2$ sorption into the clay layers. Furthermore, in this context, it is of paramount importance to better understand the photodegenerative effect of humidity, particularly of $H_2O$ in montmorillonite clay on organic compounds, as hydrated minerals are present on the martian surface and subsurface, the martian atmosphere contains significant amounts of humidity, and the existence of life is naturally associated with the presence of water. To advance our understanding of these processes, dedicated experiments spanning longer durations and varying environmental parameters are essential. Precisely tracking the photokinetic decay pathways of alanine and the temperature-dependent $CO_2$ desorption rate of the organoclay necessitates the study of gaseous products. Achieving this requires sample containers with extremely low leak rates to ensure long-term capture of gases over several months, along with stringent measures to avoid atmospheric sample contamination, giving rise to humidity-induced photodegradation. Additionally, maintaining precise temperature control at the sample locations is of paramount importance to prevent temperature-induced decomposition of organic samples. These findings from *EXPOSE-R2* have the potential to, for example, inform design concepts for Mars sample return campaigns and play a crucial role in shaping future space exposure experiments. For instance, experiments such as *OREOcube* and *Exocube*, scheduled for launch in 2025, will enable *in situ* spectroscopy of biosignatures inside hermetically sealed sample containers with simultaneous active temperature control and sample return after exposure on the ISS (Elsaesser et al., 2014; Sgambati et al., 2020).

## Authors' Contributions

S.W.: Methodology, software, validation, formal analysis, investigation, resources, data curation, writing—original draft, and visualization. P.M.: Software and formal analysis. R.G.U.: Software, formal analysis, and writing—review and editing. S.W.: Methodology, investigations, and resources. A.S.: Investigations and resources. A.J.R.: Conceptualization and writing—review and editing. R.C.Q.: Conceptualization and writing—review and editing. A.L.M.: Conceptualization and writing—review and editing. N.C.J.: Resources, formal analysis, and writing—review and editing. S.V.H.: Resources and writing—review and editing. H.C.: Project administration, resources, and writing—review and editing. D.C.: Project administration and resources. P.E.: Project administration, conceptualization, supervision, and writing—review and editing. A.E.: Conceptualization,

supervision, investigation, resources, methodology, software, project administration, and writing—review and editing.

### Author Disclosure Statement

All authors declare that they have no conflict of interest.

### Funding Information

A.E. and P.M. were supported by the Volkswagen Foundation and its Freigeist Program. A.E., S.Wi, and S.Wo. were also supported by the Ministry of Economics and Energy (Projekträger Deutsches Zentrum für Luft-und Raumfahrt, grants 50WB1623, 50WB2023 and 50WB2323). Furthermore, A.E. and R.G.U. were funded by the Einstein Foundation Berlin (IPF-2018–469). P.E. and A.E. received funding from the Nederlandse Organisatie voor Wetenschappelijk Onderzoek (NWO, grant number GO-MG/13), which is gratefully acknowledged. H.C. received funding from CNES (Centre National d'Etudes Spatiales).

### Supplementary Material

Supplementary Figure S1
Supplementary Figure S2
Supplementary Figure S3
Supplementary Figure S4
Supplementary Figure S5
Supplementary Figure S6
Supplementary Figure S7
Supplementary Table S1
Supplementary Table S2
Supplementary Table S3

### References

Azzouz A, Nousir S, Platon N, et al. Truly reversible capture of $CO_2$ by montmorillonite intercalated with soya oil-derived polyglycerols. *International Journal of Greenhouse Gas Control* 2013;17:140–147; doi: 10.1016/j.ijggc.2013.04.013

Banin A, Lawless JG, Mazzurco J, et al. pH Profile of the Adsorption of Necleotides onto Montmorillonite. *Origins Life Evol Biosphere* 1985;15(2):89–101.

Baratta GA, Accolla M, Chaput D, et al. Photolysis of cometary organic dust analogs on the EXPOSE-R2 mission at the international space station. *Astrobiology* 2019;19(8):1018–1036; doi: 10.1089/ast.2018.1853

Barnes JW, Turtle EP, Trainer MG, et al. Science goals and objectives for the dragonfly titan rotorcraft relocatable lander. *Planetary Science Journal* 2021;2(4); doi: 10.3847/PSJ/abfdcf

Berger T, Przybyla B, Matthiä D, et al. DOSIS & DOSIS 3D: Long-term dose monitoring onboard the columbus laboratory of the international space station (ISS). *J Space Weather Space Clim* 2016;6:A39; doi: 10.1051/swsc/2016034

Bertie JE, Morrison MM. The infrared spectra of the hydrates of ammonia, NH3·H2O and 2NH3·H2O at 95 °K. *The Journal of Chemical Physics* 1980;73(10):4832–4837; doi: 10.1063/1.440002

Bertrand M, Chabin A, Brack A, et al. The PROCESS experiment: Exposure of amino acids in the EXPOSE-E experiment on the international space station and in laboratory simulations. *Astrobiology* 2012;12(5):426–435; doi: 10.1089/ast.2011.0755

Bertrand M, Chabin A, Colas C, et al. The AMINO experiment: Exposure of amino acids in the EXPOSE-R experiment on the international space station and in laboratory. International Journal of Astrobiology 2015;14(1):89–97; doi: 10.1017/s1473550414000354

Bhartia R, Beegle LW, DeFlores L, et al. Perseverance's scanning habitable environments with raman and luminescence for organics and chemicals (SHERLOC) investigation. *Space Sci Rev* 2021;217(4); doi: 10.1007/s11214-021-00812-z

Bish DL, Blake DF, Vaniman DT, et al; MSL Science Team. X-ray diffraction results from mars science laboratory: Mineralogy of rocknest at gale crater. *Science* 2013;341(6153):1238932–1238935; doi: 10.1126/science.1238932

Böttger U, de Vera JP, Fritz J, et al. Optimizing the detection of carotene in cyanobacteria in a martian regolith analogue with a Raman spectrometer for the ExoMars mission. *Planetary and Space Science* 2012;60(1):356–362; doi: 10.1016/j.pss.2011.10.017

Bowles J, Jähnigen S, Agostini F. Influence-of-the-environment-on-the-infrared-spectrum-of-alanine-an-effective-modes-analysis. ChemRxiv 2022; doi: 10.1063/5.0135608

Brack A. Clay Minerals and the Origin of Life. In: Handbook of Clay Science. 2013; pp. 507–521.

Bu HL, Yuan P, Liu HM, et al. Formation of macromolecules with peptide bonds via the thermal evolution of amino acids in the presence of montmorillonite: Insight into prebiotic geochemistry on the early Earth. *Chemical Geology* 2019;510:72–83; doi: 10.1016/j.chemgeo.2019.02.023

Bumay SG, Nelson K. Leakage of Transport Container Seals During Slow Thermal Cycling to −40°C. International Journal of Radioactive Materials Transport 1991;2(1–3):91–96; doi: 10.1179/rmt.1991.2.1-3.91

Busch A, Bertier P, Gensterblum Y, et al. On sorption and swelling of CO2 in clays. *Geomech Geophys Geo-Energ Geo-Resour* 2016;2(2):111–130; doi: 10.1007/s40948-016-0024-4

Cao XL, Fischer G. Infrared spectra of monomeric L-alanine and L-alanine-N-$d_3$ zwitterions isolated in a KBr matrix. *Chemical Physics* 2000;255(2–3):195–204; doi: 10.1016/S0301-0104(00)00082-3

Caroline ML, Sankar R, Indirani RM, et al. Growth, optical, thermal and dielectric studies of an amino acid organic nonlinear optical material: L-Alanine. *Materials Chemistry and Physics* 2009;114(1):490–494; doi: 10.1016/j.matchemphys.2008.09.070

Carrier BL, Abbey WJ, Beegle LW, et al. Attenuation of ultraviolet radiation in rocks and minerals: Implications for mars science. JGR Planets 2019;124(10):2599–2612; doi: 10.1029/2018je005758

Chyba C, Sagan C. Endogenous production, exogenous delivery and impact-shock synthesis of organic molecules: An inventory for the origins of life. *Nature* 1992;355:125–132; doi: 10.1038/355125a0

Cottin H, Kotler JM, Billi D, et al. Space as a tool for astrobiology: Review and recommendations for experimentations in earth orbit and beyond. *Space Sci Rev* 2017;209(1–4):83–181; doi: 10.1007/s11214-017-0365-5

Cottin H, Rettberg P. EXPOSE-R2 on the international space station (2014-2016): Results from the PSS and BOSS astrobiology experiments. Astrobiology. Astrobiology 2019;19(8):975–978; doi: 10.1089/ast.2019.0625

Cronin JR, Pizzarello S. Enantiomeric excesses in meteoritic amino acids. Science 1997;275(5302):951–955.

Cruz-Diaz GA, Ricca A, Mattioda AL. Polycyclic aromatic hydrocarbons and dust particle surface interactions: Catalytic hydrogenation of polycyclic aromatic hydrocarbon molecules under vacuum conditions. *ACS Earth Space Chem* 2020; 4(10):1730–1742; doi: 10.1021/acsearthspacechem.0c00145

Dartnell LR. Ionizing radiation and life. *Astrobiology* 2011; 11(6):551–582; doi: 10.1089/ast.2010.0528

Jang SD, Condrare RA. Sr., Infrared Spectra of alpha-Alanine Adsorbed on Cu-Montmorillonite. Appl Spectrosc 1972; 26(1):102–104.

dos Santos R, Patel M, Cuadros J, et al. Influence of mineralogy on the preservation of amino acids under simulated Mars conditions. *Icarus* 2016;277:342–353; doi: 10.1016/j.icarus.2016 .05.029

Ehrenfreund P, Bernstein MP, Dworkin JP, et al. The photostability of amino acids in space. *Astrophysical Journal* 2001; 550(1):L95–L99; doi: 10.1086/319491

Ehrenfreund P, Ricco AJ, Squires D, et al. The O/OREOS mission-Astrobiology in low Earth orbit. *Acta Astronautica* 2014;93:501–508; doi: 10.1016/j.actaastro.2012.09.009

Elsaesser A, Quinn RC, Ehrenfreund P, et al. Organics exposure in orbit (OREOcube): A next-generation space exposure platform. *Langmuir* 2014;30(44):13217–13227; doi: 10.1021/ la501203g

Enya K, Yamagishi A, Kobayashi K, et al. Comparative study of methods for detecting extraterrestrial life in exploration mission of Mars and the solar system. *Life Sci Space Res (Amst)* 2022;34:53–67; doi: 10.1016/j.lssr.2022.07.001

Ferris JP. Montmorillonite-catalysed formation of RNA oligomers: The possible role of catalysis in the origins of life. *Philos Trans R Soc Lond B Biol Sci* 2006;361(1474): 1777–1786; discussion 1786; doi: 10.1098/rstb.2006.1903

Friebele E, Shimoyama A, Ponnamperuma C. Adsorption of protein and non-protein amino acids on a clay mineral: A possible role of selection in chemical evolution. *J Mol Evol* 1980;16(3–4):269–278; doi: 10.1007/BF01804978

Frinak EK, Mashburn CD, Tolbert MA, et al. Infrared characterization of water uptake by low-temperature Na-montmorillonite: Implications for Earth and Mars. J Geophys Res 2005; 110(D9); doi: 10.1029/2004jd005647

Garcia AR, de Barros RB, Lourenco JP, et al. The infrared spectrum of solid L-alanine: Influence of pH-induced structural changes. *J Phys Chem A* 2008;112(36):8280–8287; doi: 10 .1021/jp802170n

Gauger T, Konhauser K, Kappler A. Protection of phototrophic iron(II)-oxidizing bacteria from UV irradiation by biogenic iron(III) minerals: Implications for early archean banded iron formation. *Geology* 2015;43(12):G37095.1–G1070; doi: 10 .1130/G37095.1

Glaze LS, Wilson CF, Zasova LV, et al. Future of Venus Research and Exploration. *Space Sci Rev* 2018;214(5); doi: 10.1007/s11214-018-0528-z

Grasset O, Dougherty MK, Coustenis A, et al. JUpiter ICy moons Explorer (JUICE): An ESA mission to orbit Ganymede and to characterise the Jupiter system. *Planetary and Space Science* 2013;78:1–21; doi: 10.1016/j.pss.2012.12.002

Hassler DM, Zeitlin C, Wimmer-Schweingruber RF, et al; MSL Science Team. Mars' surface radiation environment measured with the Mars Science Laboratory's Curiosity rover. *Science* 2014;343(6169):1244797; doi: 10.1126/science.1244797

Higgs PG, Pudritz RE. A thermodynamic basis for prebiotic amino acid synthesis and the nature of the first genetic code. *Astrobiology* 2009;9(5):483–490; doi: 10.1089/ast.2008.0280

Hill DJT, O'Donnell JH, Pomery PJ, et al. Photolysis of Poly(amino acid)s at 77 K: An ESR Study. *Polymer Degradation and Stability* 1985;10(1):15–23; doi: 10.1016/0141-3910(85)90017-5

Howell SM, Pappalardo RT. NASA's Europa Clipper-a mission to a potentially habitable ocean world. *Nat Commun* 2020; 11(1):1311; doi: 10.1038/s41467-020-15160-9

Iglesias-Groth S, Cataldo F. Integrated molar absorptivity of mid- and far-infrared spectra of alanine and a selection of other five amino acids of astrobiological relevance. *Astrobiology* 2022;22(4):462–480; doi: 10.1089/ast.2021.0094

Johnson PV, Hodyss R, Chernow VF, et al. Ultraviolet photolysis of amino acids on the surface of icy Solar System bodies. *Icarus* 2012;221(2):800–805; doi: 10.1016/j.icarus.2012.09 .005

Kamei S, Hibi J, Ohtsubo Y, et al. Infrared evaluation of enantiometric amount and application to racemization at the interface between L- and D-Alanine. *Appl Spectrosc* 2018;72(7): 1074–1079; doi: 10.1177/0003702818770575

Kloprogge JTT, Hartman H. Clays and the origin of life: The experiments. *Life (Basel)* 2022;12(2); doi: 10.3390/life12020259

Kochanov RV, Gordon IE, Rothman LS, et al. HITRAN application programming interface (HAPI): A comprehensive approach to working with spectroscopic data. *Journal of Quantitative Spectroscopy & Radiative Transfer* 2016;177: 15–30; doi: 10.1016/j.jqsrt.2016.03.005

Kogel JE, Lewis SA. Baseline studies of the clay minerals society source clays: Chemical analysis by inductively coupled plasma-mass spectrscopy (ICP-MS). *Clays and Clay Miner* 2001;49(5):387–392.

Kopacz N, Corazzi MA, Poggiali G, et al. The photochemical evolution of polycyclic aromatic hydrocarbons and nontronite clay on early Earth and Mars. *Icarus* 2023;394:115437; doi: 10.1016/j.icarus.2023.115437

Kozak M, Domka L. Adsorption of the quaternary ammonium salts on montmorillonite. *Journal of Physics and Chemistry of Solids* 2004;65(2–3):441–445; doi: 10.1016/j.jpcs.2003.09 .015

Kuligiewicz A, Derkowski A, Szczerba M, et al. Revisiting the infrared spectrum of the water-smectite interface. *Clays and Clay Miner* 2015;63(1):15–29; doi: 10.1346/Ccmn .2015.0630102

Liu D, Kounaves SP. Degradation of amino acids on mars by uv irradiation in the presence of chloride and oxychlorine salts. *Astrobiology* 2021;21(7):793–801; doi: 10.1089/ast.2020 .2328

MacKenzie SM, Neveu M, Davila AF, et al. The enceladus orbilander mission concept: Balancing return and resources in the search for life. *Planetary Science Journal* 2021;2(2); doi: 10 .3847/PSJ/abe4da

Mancinelli RL, Klovstad M. Martian soil and UV radiation: Microbial viability assessment on spacecraft surfaces. *Planetary and Space Science* 2000;48(11):1093–1097; doi: 10 .1016/S0032-0633(00)00083-0

Marschall M, Dulai S, Kereszturi A. Migrating and UV screening subsurface zone on Mars as target for the analysis of photosynthetic life and astrobiology. *Planetary and Space Science* 2012;72(1):146–153; doi: 10.1016/j.pss.2012.05.019

Martin RT. Data handbook for clay materials and other nonmetallic minerals. *Clays and Clay Miner* 1980;28(2):160–160; doi: 10.1346/ccmn.1980.0280215

Mate B, Rodriguez-Lazcano Y, Galvez O, et al. An infrared study of solid glycine in environments of astrophysical relevance. *Phys Chem Chem Phys* 2011;13(26):12268–12276; doi: 10.1039/c1cp20899c

Maté B, Tanarro I, Escribano R, et al. Stability of extraterrestrial glycine under energetic particle radiation estimated from 2 keV electron bombardment experiments. *ApJ* 2015;806(2): 151; doi: 10.1088/0004-637x/806/2/151

Mattioda A, Cook A, Ehrenfreund P, et al. The O/OREOS mission: First science data from the space environment viability of organics (SEVO) payload. *Astrobiology* 2012;12(9): 841–853; doi: 10.1089/ast.2012.0861

Max J-J, Chapados C. Aqueous ammonia and ammonium chloride hydrates: Principal infrared spectra. *Journal of Molecular Structure* 2013;1046:124–135; doi: 10.1016/j.molstruc .2013.04.045

Mendel N, Sîretanu D, Sîretanu I, et al. Interlayer Cation-Controlled Adsorption of Carbon Dioxide in Anhydrous Montmorillonite Clay. *J Phys Chem C* 2021;125(49): 27159–27169; doi: 10.1021/acs.jpcc.1c06746

Michels L, Fossum JO, Rozynek Z, et al. Intercalation and retention of carbon dioxide in a smectite clay promoted by interlayer cations. *Sci Rep* 2015;5:8775; doi: 10.1038/ srep08775

Minkov VS, Chesalov YA, Boldyreva EV. A Study of the temperature effect on the ir spectra of crystalline amino acids, dipetids, and polyamino acids. *J Struct Chem* 2010;51(6): 1052–1063; doi: 10.1007/s10947-010-0162-4

Modica P, Meinert C, de Marcellus P, et al. Enantiomeric excesses induced in amino acids by ultraviolet circularly polarized light irradiation of extraterrestrial ice analogs: A possible source of asymmetry for prebiotic chemistry. *ApJ* 2014;788(1):79; doi: 10.1088/0004-637x/788/1/79

Mohamed ME, Mohammed AMA. Experimental and computational vibration study of amino acids. *Ilcpa* 2013;15:1–17; doi: 10.56431/p-177d2l

Moore B, Toh SY, Wong YTA, et al. Hydrocarboxyl radical as a product of alpha-alanine ultraviolet photolysis. *J Phys Chem Lett* 2021;12(50):11992–11997; doi: 10.1021/acs .jpclett.1c03104

Moores JE, Smith PH, Tanner R, et al. The shielding effect of small-scale martian surface geometry on ultraviolet flux. *Icarus* 2007;192(2):417–433; doi: 10.1016/j.icarus.2007.07.003

Morris RV, Klingelhöfer G, Bernhardt B, et al. Mineralogy at gusev crater from the moessbauer spectrometer on the spirit rover. *Science* 2004;305(5685):833–836; doi: 10.1126/ science.1100020

Mortland M, Fripiat J, Chaussidon J, et al. Interaction between ammonia and the expanding lattices of montmorillonite and vermiculite. *J Phys Chem* 1963;67(2):248–258; doi: 10.1021/ j100796a009

Mortland MM. Clay-Organic Complexes and Interactions. Advances in Agronomy 1970;22:75–117; doi: 10.1016/ S0065-2113(08)60266-7

Murchie SL, Mustard JF, Ehlmann BL, et al. A synthesis of Martian aqueous mineralogy after 1 Mars year of observations from the Mars Reconnaissance Orbiter. J Geophys Res 2009;114(E2); doi: 10.1029/2009je003342

Nazdracheva T, Morozov A, Yavna V, et al. Study of hydration of kaolinite and montmorillonite mixture by IR spectroscopy. *Journal of Molecular Structure* 2022;1250:131871; doi: 10 .1016/j.molstruc.2021.131871

Oró J, Holzer G. The photolytic degradation and oxidation of organic compounrs under simulated martian conditions. *J Mol Evol* 1979;14(1–3):153–160; doi: 10.1007/BF01732374

Parnell J, Cullen D, Sims MR, et al. Searching for life on Mars: Selection of molecular targets for ESA's aurora ExoMars mission. *Astrobiology* 2007;7(4):578–604; doi: 10.1089/ast .2006.0110

Pilling S, Nair BG, Escobar A, et al. The temperature effect on the glycine decomposition induced by 2 keV electron bombardment in space analog conditions. *European Physical Journal D* 2014;68(3); doi: 10.1140/epjd/e2014-40739-9

Poch O, Kaci S, Stalport F, et al. Laboratory insights into the chemical and kinetic evolution Of several organic molecules under simulated Mars surface UV radiation conditions. *Icarus* 2014;242:50–63; doi: 10.1016/j.icarus.2014.07.014

Primm KM, Gough V, Wong J, et al. The effect of mars-relevant soil analogs on the water uptake of magnesium perchlorate and implications for the near-surface of mars. JGR Planets 2018;123(8):2076–2088; doi: 10.1029/2018je005540

Rabbow E, Rettberg P, Barczyk S, et al. The astrobiological mission EXPOSE-R on board of the International Space Station. International Journal of Astrobiology 2015;14(1):3–16; doi: 10.1017/s1473550414000202

Rabbow E, Rettberg P, Barczyk S, et al. EXPOSE-E: An ESA astrobiology mission 1.5 years in space. *Astrobiology* 2012; 12(5):374–386; doi: 10.1089/ast.2011.0760

Rabbow E, Rettberg P, Parpart A, et al. EXPOSE-R2: The astrobiological esa mission on board of the international space station. *Front Microbiol* 2017;8:1533; doi: 10.3389/fmicb.2017 .01533

Rak J, Chomicz L, Wiczk J, et al. Mechanisms of damage to dna labeled with electrophilic nucleobases induced by ionizing or UV radiation. *J Phys Chem B* 2015;119(26): 8227–8238; doi: 10.1021/acs.jpcb.5b03948

Rodríguez-Lazcano Y, Maté B, Galvez O, et al. Solid L-alpha-alanine: Spectroscopic properties and theoretical calculations. *Journal of Quantitative Spectroscopy and Radiative Transfer* 2012;113(11):1266–1275; doi: 10.1016/j.jqsrt.2012.01.020

Romanov VN. Evidence of irreversible $CO_2$ intercalation in montmorillonite. *International Journal of Greenhouse Gas Control* 2013;14:220–226; doi: 10.1016/j.ijggc.2013.01.022

Rosado MTS, Duarte MLRS, Fausto R. Vibrational Spectra (FT-IR, Raman and MI-IR) of alpha- and beta-alanine. Journal of Molecular Structure 1997;410–411:343–348; doi: 10 .1016/S0022-2860(96)09695-0

Rossi AP, van Gasselt S. Geology of Mars after the first 40 years of exploration. *Res Astron Astrophys* 2010;10(7):621–652; doi: 10.1088/1674-4527/10/7/003

Rozenberg M, Shoham G, Reva I, et al. Low-temperature Fourier transform infrared spectra and hydrogen bonding in polycrystalline L-alanine. *Spectrochim Acta A Mol Biomol Spectrosc* 2003;59(14):3253–3266; doi: 10.1016/s1386-1425(03)00159-8

Russell JD. Infra-red study of the reactions of ammonia with montmorillonite and saponite. *Trans Faraday Soc* 1965;61: 2284–2294; doi: 10.1039/TF9656102284

Ryan CG, Clayton E, Griffin WL, et al. Snip, a statistics-sensitive background treatment for the quantitative-analysis

of pixe spectra in geoscience applications. *Nuclear Instruments & Methods in Physics Research Section B-Beam Interactions with Materials and Atoms* 1988;34(3):396–402; doi: 10.1016/0168-583x(88)90063-8

Sagstuen E, Sanderud A, Hole EO. The solid-state radiation chemistry of simple amino acids, revisited. *Radiat Res* 2004; 162(2):112–119; doi: 10.1667/rr3215

Salam H, Davies I. Development of biobased polymer/clay nanocomposites: A critical review. In: Fillers and Reinforcements for Advanced Nanocomposites. Woodhead Publishing Series: 2015; pp. 101–132.

Sephton MA, Carter JN. The chances of detecting life on Mars. *Planetary and Space Science* 2015;112:15–22; doi: 10.1016/j .pss.2015.04.002

Sgambati A, Deiml M, Stettner A, et al. SPECTROModule: A modular spectroscopy platform for exobiology and space sciences. *Acta Astronautica* 2020;166:377–390; doi: 10.1016/j .actaastro.2019.10.010

Stalport F, Rouquette L, Poch O, et al. The Photochemistry on Space Station (PSS) Experiment: Organic Matter under Mars-like Surface UV Radiation Conditions in Low Earth Orbit. *Astrobiology* 2019;19(8):1037–1052; doi: 10.1089/ast .2018.2001

Kate IL, Garry JRC, Peeters Z, et al. Amino acid photostability on the Martian surface. *Meteoritics & Planetary Science* 2005; 40(8):1185–1193; doi: 10.1111/j.1945-5100.2005.tb00183.x

Uddin F. Clays, Nanoclays, and Montmorillonite Minerals. Metall Mater Trans A 2008;39(12):2804–2814; doi: 10.1007/s11661-008-9603-5

Valaskova M, Martynkova GS. Clay Minerals in Nature - Their Characterization, Modification and Application, Chapter 10: Role of Clay Minerals in Chemical Evolution and the Origins of Life. 2012.

Venyaminov SY, Prendergast FG. Water (H2O and D2O) molar absorptivity in the 1000-4000 cm(-1) range and quantitative infrared spectroscopy of aqueous solutions. *Anal Biochem* 1997;248(2):234–245; doi: 10.1006/abio.1997.2136

Wang H, Agmon N. Complete assignment of the infrared spectrum of the gas-phase protonated ammonia dimer. *J Phys Chem A* 2016;120(19):3117–3135; doi: 10.1021/acs.jpca .5b11062

Wernicke LJ, Jakosky BM. Martian hydrated minerals: A significant water sink. JGR Planets 2021;126(3); doi: 10.1029/ 2019JE006351

Yeşilbaş M, Holmboe M, Boily J-F. Residence times of nanoconfined $CO_2$ in layered aluminosilicates. *Environ Sci: Nano* 2019;6(1):146–151; doi: 10.1039/c8en01156g

Yeşilbaş M, Holmboe M, Boily J-F. Cohesive vibrational and structural depiction of intercalated water in montmorillonite. *ACS Earth Space Chem* 2018;2(1):38–47.

Zheng WJ, Jewitt D, Kaiser RI. Infrared Spectra of Ammonia-Water Ices. *ApJS* 2009;181(1):53–61; doi: 10.1088/0067-0049/181/1/53

Address correspondence to:
*Andreas Elsaesser*
*Experimental Biophysics and Space Sciences*
*Department of Physics*
*Freie Universitaet Berlin*
*Arnimallee 14*
*14195 Berlin*
*Germany*

*E-mail:* a.elsaesser@fu-berlin.de

Submitted March 19, 2024
Accepted January 8, 2025
Associate Editor: Petra Rettberg

**Abbreviations Used**

| | |
|---|---|
| $CO_2$ | = carbon dioxide |
| D–alanine | = dextrorotatory alanine |
| DLR | = German Aerospace Center (Deutsches Zentrum für Luft- und Raumfahrt |
| FTIR | = Fourier-transform infrared |
| ISS | = International Space Station |
| L–alanine | = levorotatory alanine |
| LEO | = low Earth orbit |
| $MgF_2$ | = magnesium fluoride |
| MMNT | = montmorillonite |
| MUSC | = Microgravity User Support Center |
| PSS | = Photochemistry on the Space Station |
| Rac–alanine | = racemic alanine |
| UV | = ultraviolet |